Published in final edited form as:
Nature. 2016 February 18; 530(7590): 344–348. doi:10.1038/nature16953.

The sexual identity of adult intestinal stem cells controls organ size and plasticity

Bruno Hudry[1,2], **Sanjay Khadayate**[1], and **Irene Miguel-Aliaga**[1,2]

[1]MRC Clinical Sciences Centre, Imperial College London, Hammersmith Campus, Du Cane Road, London W12 0NN

SUMMARY

Sex differences in physiology and disease susceptibility are commonly attributed to developmental and/or hormonal factors, but there is increasing realisation that cell-intrinsic mechanisms play important and persistent roles[1,2]. Here we use the *Drosophila melanogaster* intestine to investigate the nature and significance of cellular sex in an adult somatic organ *in vivo*. We find that the adult intestinal epithelium is a cellular mosaic of different sex differentiation pathways, and displays extensive sex differences in expression of genes with roles in growth and metabolism. Cell-specific reversals of the sexual identity of adult intestinal stem cells uncover its key roles in controlling organ size, its reproductive plasticity and its response to genetically induced tumours. Unlike previous examples of sexually dimorphic somatic stem cell activity, the sex differences in intestinal stem cell behaviour arise from intrinsic mechanisms, which control cell cycle duration and involve a new *doublesex*- and *fruitless*-independent branch of the sex differentiation pathway downstream of *transformer*. Together, our findings indicate that the plasticity of an adult somatic organ is reversibly controlled by its sexual identity, imparted by a new mechanism that may be active in more tissues than previously recognised.

Sex differences in intestinal physiology[3] prompted us to investigate possible molecular underpinnings. RNA-seq transcriptional profiling of virgin adult midguts (GEO accession number GSE74775) indicated significant sexual dimorphism in gene expression and/or splicing, with 8.3% of all genes and 5.6% of all isoforms expressed in the midgut displaying sex differences in expression (Extended Data Fig. 1a-f and GutSexRNAseq.xls). Sex-biased expression or splicing was confirmed for a subset of genes by real time qRT-PCR (Extended Data Fig. 1h, i). Genes with sex differences in expression cluster into distinct biological processes; genes assigned to cell division-related processes are more abundantly expressed in females, whereas genes coding for proteins that function in carbohydrate metabolism and redox processes are preferentially expressed in males (Extended Data Fig. 1g).

[2]Authors for correspondence: i.miguel-aliaga@imperial.ac.uk (IM-A); bruno.hudry@imperial.ac.uk (BH).

Authors contributions

B.H. and I.M-A. designed and conceived the study. S.K. performed statistical analyses of RNA-seq data, B.H. performed all other experiments in the study and analysed data. I.M-A. analysed data and wrote the manuscript, with contributions from B.H.

Competing financial interests

The authors have no competing financial interests.

Europe PMC Funders Author Manuscripts

The above results suggested active expression of sex determinants in the adult intestine. In *Drosophila*, sex chromosome sensing leads to sexually dimorphic expression of *Sex lethal* (*Sxl*): the master regulator of both sexual development and dosage compensation (DC, an epigenetic process by which transcription of the single male X chromosome is upregulated twofold[4]). *Sxl* controls the sex-specific splicing of its downstream target gene *transformer* (*tra*)[5], leading to functional Tra protein expression only in females, and to the sex-specific splicing of two Tra direct targets – the transcription factors *doublesex* (*dsx*) and *fruitless* (*fru*) – that sculpt sexually dimorphic anatomical features, reproductive systems and behaviour[6-8] (Extended Data Fig. 2b). As may be expected from their roles in DC[4], Sxl and the sexually dimorphic DC complex (DCC) member Male-specific lethal 2 (Msl-2) are ubiquitously expressed in the intestinal epithelium of females and males, respectively, in both adult intestinal progenitors (intestinal stem cells (ISCs) and postmitotic enteroblasts (EBs)) and their differentiated progeny (enterocytes (ECs) and enteroendocrine cells (EECs)) (Extended Data Fig. 2a-d). Consistent with our RNA-seq analysis, a newly generated *tra-LacZ* reporter is also expressed in all four epithelial cell types of the adult intestine (Extended Data Fig. 2a, e) - suggesting that, downstream of Sxl, the sex differentiation pathway remains active in this adult epithelium. However, the two targets of Tra-mediated sex-specific splicing are either absent from all midgut epithelial cells (Fru^M), or are expressed in only a subset of epithelial cells ($Dsx^{F/M}$, expressed in ECs but absent from ISCs, EBs and EECs) (Extended Data Fig. 2a, f, g). Hence, the expression of sex determination genes is maintained in the adult midgut, but displays cell type specificity; while adult-born enterocytes express all members of the canonical sex determination pathway, their siblings (the EECs) and both types of adult intestinal progenitors (ISCs and EBs) express the early (Sxl, Tra), but not the late ($Dsx^{F/M}$, Fru^M), effectors of the pathway.

Both the enrichment analysis and the presence of Sxl/*tra* in adult ISCs pointed to sexually dimorphic ISC proliferation. Female flies exhibit a rapid proliferative response to dextran sodium sulphate (DSS)-induced damage of the intestinal epithelium (Fig. 1a and [9]). This response was less pronounced in male midguts (Fig. 1a), or in female (but not male) midguts following adult-restricted *Sxl* downregulation in intestinal progenitors (Fig. 1a and Extended Data Fig. 3a, c). Conversely, ectopic expression of *Sxl* in adult intestinal progenitors enhanced proliferation in male (but not female) midguts (Fig. 1a and Extended Data Fig. 3a). Additional cell type- and adult-specific *Sxl* downregulation experiments indicated that *Sxl* acts in ISCs, and not in other cells, to control sexually dimorphic proliferation rather than differentiation (Fig. 1e and Extended Data Figs. 3d and 4a). Mechanistically, females do not have a significantly higher density of ISCs than male flies (Fig. 1b) or a higher ratio of symmetric vs asymmetric divisions (Fig. 1c), suggesting that the proliferative capacity of female ISCs is intrinsically enhanced by their expression of Sxl. Consistent with this idea, a higher percentage of their adult progenitors are found in G2/S phase at the expense of G1 during in homeostatic conditions (Fig. 1d), suggestive of shorter cell cycles, and adult-specific downregulation of *Sxl* in intestinal progenitors abrogated the sexual dimorphism in G2/S to G1 ratio, without affecting the number of ISCs or their division mode (Figs. 1b-d). Clonal analyses further confirmed the intrinsic nature of the sexual dimorphism in proliferation, its Sxl control and adult reversibility both during regeneration and homeostasis (Fig. 1g and Extended Data Fig. 3b, e and f).

To investigate whether the reported Sxl effects result from deregulated DC, we first confirmed that DC can be functionally inactivated in adults by observing loss of histone H4 lysine 16 acetylation of the X chromosome upon adult-specific downregulation of *msl-2* in male intestinal progenitors (Extended Data Fig. 3g). We then investigated whether ectopic *msl-2* expression accounted for the reduced proliferation resulting from *Sxl* downregulation by co-downregulating both genes in adult intestinal progenitors. This did not reinstate female proliferation (Fig. 1f). The converse experiment - mis-expression of *msl-2* in adult female intestinal progenitors using a newly generated transgene coding for HA-tagged Msl-2 - did not reduce their proliferation (Fig. 1f) despite efficient Msl-2 protein expression and function (Extended Data Fig. 3h and data not shown). Hence, DC does not account for the ISC sex differences.

This focused our attention on the sex differentiation pathway and its main effector *tra*. Like *Sxl*, *tra* downregulation reduced DSS-induced proliferation in females to levels comparable to those seen in male midguts, but did not affect proliferation in male midguts (Fig. 2a and Extended Data Fig. 5a). Conversely, *tra* mis-expression – either ubiquitous (Extended Data Fig. 5c) or confined to adult intestinal progenitors (Fig. 2a and Extended Data Fig. 5a) - increased the proliferative response of ISCs to DSS in adult males, but not in females. Clonal and *tra* mutant rescue experiments further confirmed the adult, cell-intrinsic requirement for *tra* in regulating sexually dimorphic proliferation, both during regeneration (Extended Data Fig. 5b, d) and in normal homeostasis (Fig. 2c and Extended Data Fig. 5e, f). Strikingly, reintroduction of a *tra* transgene specifically in adult intestinal progenitors fully rescued the reduced proliferation resulting from *Sxl* downregulation (Fig. 2b). Together with the *Sxl* experiments, these results show that the sex of the midgut is actively specified in adult flies. Unlike other adult somatic cell types[6,10,11], adult ISCs have a plastic sexual identity manifested by an intrinsic, *Sxl/tra*-controlled and DC-independent sexual dimorphism in both their basal and regenerative proliferation. These findings extend previous work in both mouse and *Drosophila*[12-16] by showing that sexual identity not only needs to be actively maintained, but can also be reversed bidirectionally in the adult cells of a nongonadal organ.

Unexpectedly (and in contrast to *tra*), mutation of the canonical Tra binding partner Transformer 2 (Tra2)[5,7] failed to affect the sex differences in ISC proliferation (Fig. 2d), despite interfering with the sex-specific expression of dsx^F and Yolk protein 1 (Yp1) transcripts as anticipated (Extended Data Fig. 5g). Together with our finding that ISCs do not express Dsx or Fru^M (Extended Data Fig. 2a, f, g), this result suggested that a non-canonical Tra2-, Dsx-, Fru^M-independent sex determination pathway drives sexually dimorphic proliferation in adult intestinal stem cells. We conducted a series of rescue, gain- and loss-of-function experiments using dsx^F transgenes, *dsx*/*fru* mutants, RNAi transgenes and mutants in which *dsx*/*fru* splicing was biased towards either male or female isoforms (Extended Data Fig. 6a-g). These ruled out both a direct action of *dsx* or fru^M in intestinal progenitors as well as indirect contributions to ISC proliferation from other dsx/fru^M-expressing cells such as the neighbouring ECs, thus confirming that the sex of adult somatic stem cells in the intestine is specified by a novel branch of the sex determination pathway.

We then combined new RNA-seq and genetic experiments to identify *tra* target genes in adult ISCs, defined as genes the expression or splicing of which was different between control and *tra* mutant females, but returned to levels comparable to those of controls upon adult ISC-specific re-introduction of *tra* (see Methods, GEO accession number GSE74775 and GutSexRNAseq.xls for details). This yielded 72 genes with *tra*-regulated expression (34) or splicing (38) (Fig. 3a, b and Extended Data Fig. 7a-c). A genetic screen (Extended Data Fig. 7d, see Methods for details) identified three of them as negative or positive regulators of proliferation accounting for the sexual dimorphism in ISC proliferation. Indeed, downregulation of *Imaginal disc growth factor 1* (*Idgf1*) or *Serpin 88Eb* (*Spn88Eb*), normally activated by *tra* in adult intestinal progenitors, reduced proliferation only in females. By contrast, over-expression of *reduced ocelli* (*rdo*), normally repressed by *tra* in the same cells, reduced proliferation only in females (Fig. 3c and Extended Data Fig. 7e). These three targets are regulated at the expression – rather than splicing – level: consistent with novel, *tra2*- and, possibly, splicing-independent roles of *tra*. Once produced, they may be secreted or targeted to the cell surface[17-19], suggesting that sex differences may result from modulation of how ISCs interact with their local environment. All three proteins also appear to be expressed in other tissues and/or during development, and belong to protein families also represented in mammals: leucine-rich repeat (*rdo*), inhibitory serpins (*Spn88Eb*) and secreted glycoproteins (*Idgf1*)[17,19,20]. It will therefore be interesting to explore whether they account for how organisms attain their sexually dimorphic body size during development.

Are the sex differences in ISCs physiologically significant? Wild-type female midguts are longer than male midguts at days 3, 5 and 20 of adult life (Fig. 4a and data not shown). Adult-specific and cell-autonomous masculinisation of ISCs (achieved by *tra* or *Sxl* downregulation) dramatically shrank the female (but not the male) midgut towards a male-like size (Fig. 4a and Extended Data Fig. 8c). Cell type- and region-specific quantifications indicated that a reduction in ISC proliferation and, consequently, the number of differentiated progeny accounted for the observed shrinkage (Extended Data Fig. 8a-d). Female flies with masculinised adult ISCs also failed to undergo the recently described midgut resizing triggered by mating[21] (Fig. 4b and Extended Data Fig. 8e) and had slightly reduced fecundity (Extended Data Fig. 8f), indicating that sex differences endow females with enhanced stem cell plasticity to optimise reproduction. Females are, however, more prone to genetically induced tumours; indeed, adult-specific interference with *Notch* (*N*) or *Apc-ras* signalling, previously shown to lead to tissue overgrowth reminiscent of gastrointestinal tumours in females[22,23], resulted in hyperplasia of female (but not male) midguts (Fig. 4c, d and Extended Data Fig. 9a-f). Hyperplasia resulted from sex differences in proliferation rather than sex-specific differentiation defects (Extended Data Fig. 4b), and could be prevented by simultaneously masculinising female adult ISCs by downregulating or mutating *Sxl*/*tra*, but not *dsx* or fru^M (Fig. 4c, d and Extended Data Fig. 9a, c-g). Increased susceptibility of female flies to genetically induced tumours was also observed after mating (data not shown). Thus, the intrinsic sexual identity of adult intestinal stem cells plays key roles in adult life, both in maintaining organ size and in modulating its plasticity.

Previous observations had pointed to additional branches of the sex determination pathway[24,25]. Our discovery of this new branch has important implications for organs such

as the nervous system, where sexual identity was thought to be confined to Fru^M and/or Dsx-expressing neurons[26], and raises the possibility that every cell has a sexual identity that actively regulates its plasticity and physiology. While early sex specification in *Drosophila* differs from that of mammals, there is increasing evidence that it converges on common effectors - such as the Dsx/Dmrt family of transcription factors and their targets[12]. Hence, the recently reported sex differences in both intestinal gene expression and microbiota in the mammalian intestine[27,28] could at least partly result from similar, so far unexplored, intrinsic sex differences. Similarly, the possible contribution of the intrinsic sexual identity of adult somatic stem cells to both organ plasticity and to the well documented sex differences in susceptibility to many types of cancer[29,30] deserves further investigation.

METHODS

Fly husbandry

Fly stocks were reared on a standard cornmeal/agar diet (6.65% cornmeal, 7.15% dextrose, 5% yeast, 0.66% agar supplemented with 2.2% nipagin and 3.4 mL/L propionic acid). All experimental flies were kept in incubators at 25°C, 65% humidity and on a 12 hr light/dark cycle, except for those containing *tub-Gal80^{TS}* transgenes, which were set up at 18°C (restrictive temperature) and transferred to 29°C (permissive temperature) at the time when *Gal4* induction was required. This depended on the specific experimental requirements but typically, for loss-of-function (*RNAi*) or gain-of-function (*UAS*) experiments, flies were raised and aged as adults for 3 days at 18°C, were then shifted to 29°C to induce transgene expression, and adult midguts were dissected after 10-20 days (as indicated in each figure panel). Flies were transferred to fresh vials every 3 days and fly density was kept to a maximum of 15 flies per vial. Virgin flies were used for all experiments unless indicated otherwise.

For mutant ISC clonal analyses (MARCM clones), 3-day-old adults (raised and aged at 25°C) were heat-shocked for 1 hr at 37°C to induce clones, and were then kept at 25°C (or 29°C for MARCM RNAi clones) until dissection (10 days, 15 days or 4 weeks thereafter as indicated in each figure panel). Flies were transferred to fresh vials every 3 days.

For damage-induced regeneration assays, virgin flies were collected over 72 hrs at 18°C, and were then shifted to 29°C for 7 days on standard media. Flies were then transferred in an empty vial containing a piece of 3.75 cm × 2.5cm paper. 500mL of 5% sucrose solution (control) or 5% sucrose + 3 dextran sulfate sodium (DSS) solution was used to wet the paper, used as feeding substrate. Flies were transferred to new vial with fresh feeding paper every day for 3 days prior dissection.

For fecundity experiments, females were raised and aged as virgins for 3 days at 18°C, and were then shifted to 29°C to induce transgene expression for 10 days. Females were then mated overnight to OregonR males (10 males, 10 females per vial). Males were then removed, and single female flies were transferred individual vials every 24h for a 3-day period. Eggs were counted from the vacated vials.

Fly stocks

UAS* transgenes—UAS-Sxl*^{RNAi} (VDRC: GD 3131), *UAS-Sxl* (generated by [31]), *UAS-pon.GFP* (BDSC:42741, generated by [32]), *UAS-GFP.E2f1.*$^{1-230}$, *UAS-mRFP1.NLS.CycB.*$^{1-266}$ (BDSC: 55121, generated by [33]), *UAS-GFP* (BDSC: 35786), *UAS-Dicer2* (VDRC: 60007), *UAS-tra*^{RNAi} (BDSC: 28512, TRiP.JF03132), *UAS-tra*^{F} (BDSC: 4590, generated by [34]), *UAS-msl-2*^{RNAi} (VDRC: GD 29356), *UAS-Sxl*$^{RNAi\ 2}$ (VDRC: KK 109221), *UAS-msl-2*$^{RNAi\ 2}$ (BDSC:35390, TRiP.GL00309), *UAS-msl-2*^{HA} (this study), *UAS-dsx*^{RNAi} (BDSC: 26716, TRiP.JF02256), *UAS-dsx*^{F} (BDSC: 44223, generated by [35]), *UAS-Arr1* (generated by [36]), *UAS-rdo* (generated by [17]), *UAS-GstE4* (generated by [37]), *UAS-Notch*^{RNAi} (VDRC: KK 100002), *UAS-Sxl*$^{RNAi\ 3}$ (BDSC: 34393, TRiP.HMS00609), *UAS-tra*$^{RNAi\ 2}$ (VDRC: GD 2560), *UAS-tra*$^{RNAi\ 3}$ (NIG: 16724-R2), *UAS-fru*^{RNAi} (BDSC: 31593, TRiP.JF01182), *UAS-Notch*$^{RNAi\ 2}$ (VDRC: GD 27229), *UAS-Hairless* (generated by [38]), *UAS-N*^{intra} (generated by [39]), *UAS-sspitz* (gift from J. Treisman, generated by [40]), *UAS-Ras*^{V12}; *FRT82B* line (generated by [41]).

Mutants—*tra*^{1}*, FRT2A, fru*^{P1}*-Gal4* chromosome (generated by [42]), *FRT82b, dsx*^{1} chromosome (generated by [43]), *dsx*$^{\Delta}$*, Df(3R)*^{Exel6179} chromosome (generated by [44]), *Df(3R)dsx*^{11} (BDSC: 1865, generated by [45]), *In(3R)dsx*^{23} (BDSC: 1849, generated by [46]), *FRT82b, dsx*^{1}*, fru*$^{\Delta tra}$ chromosome (gift from B. Baker, generated by [47]), *dsx*^{1}*, fru*$^{P1\text{-}LexA}$ chromosome (gift from B. Prud'homme, generated by [48]), *tra*^{KO} (this study), *Df(3L)*$^{st\text{-}j7}$ (BDSC:5416, generated by [49]), *tra*^{1} (BDSC: 675, generated by [50]), *tra2*^{B} (BDSC: 25137, generated by [51]), *Df(2R)*^{trix} (BDSC:1896, generated by [52]), *tra2*^{ts1} (BDSC: 2413, generated by [52]), *dsx*^{D} (BDSC: 840, generated by [53], *fru*^{F} and *fru*^{M} (gift from G. Jefferis, generated by [47], *fru*$^{4\text{-}40}$ (gift from G. Jefferis, generated by [54]), *FRT82b, Df*^{RevF10} chromosome (gift from S. Bray, generated by [55]), *Su(H)*$^{\Delta 47}$*, FRT40A* chromosome (gift from S. Bray, generated by [56]), *FRT82B Apc2*^{N175K}*, Apc*^{Q8} chromosome and *hs-flp;UAS-Ras*^{V12}; *FRT82B Apc2*^{N175K}*, Apc*^{Q8} line (both generated by [41]).

Reporters and *Gal4* drivers—*Su(H)*^{GBE}*-LacZ* (generated by [57]), *esg-GFP*^{P01986} (gift from L. Jones, Flytrap), *esg-LacZ*^{k00606} (BDSC : 10359), *dsx-Gal4* (generated by [58]), *fru*^{P1}*-Gal4* (gift from G. Jefferis, generated by [59]), *esg-Gal4*^{NP7397}*, UAS-GFP, Tub-Gal80*^{TS} chromosome (gift from J. de Navascués), *Su(H)*^{GBE}*-Gal80* (generated by [60]), *Su(H)*^{GBE}*-Gal4* (generated by [61]), *mex1-Gal4* (generated by [62]), *pros*^{V1}*-Gal4* (generated by [63]), *Mvl-Gal4*^{NP2375}(Kyoto: 104178), *dsx*$^{\Delta 2}$*-Gal4* (generated by [64]), *vm-Gal4* (BDSC: 48547, GMR13B09-GAL4), *btl-Gal4* (generated by [65]), *nSyb-Gal4* (BDSC: 51941), *elav-Gal4* (BDSC: 8765), *nSyb-Gal80* (gift from J. Simpson), *stripe-Gal4* (BDSC: 26663).

MARCM stocks—FRT40A: *w, hs-flp,Tub-Gal4, UAS-GFP; tub-Gal80, FRT40A* (gift from J. de Navascués), FRT2A: *y, w, hs-flp; Tub-Gal4,UAS-GFP; Tub-Gal80, FRT2A* (gift from I. Salecker), *FRT2A* (BDSC: 1997), FRT82b: w, hs-flp; UAS-mCD8GFP, Tub-Gal4; FRT82b, Tub-Gal80 (gift from M. Vidal), *FRT82b* (BDSC:7369).

Generation of *tra*^{KO} and *tra*^{LacZ} transgenic lines

To generate the transgenic reporter of *tra* promoter activity *tra*^{LacZ}, the upstream intergenic region between *spd-2* and *tra* was cloned using the following primer pair: 5'-

AAAATCTAGAAACTAATAAAGTATATGAG-3' and 5'-AAAAGGTACCCGGAAAATGCTGGAAATTAAATGATGC-3'. PCR was performed with Q5 high-fidelity polymerase from New England Biolabs (M0491S). The PCR product was digested with XbaI and KpnI prior to cloning into the *pH-Pelican attb* vector ([66], gift from C. Thummel). The construct was sequence-verified and a transgenic line was established through ΦC-31 integrase mediated transformation (Bestgene, attP site: attP40).

The new amorphic allele of *tra*, tra^{KO}, was generated using the accelerated homologous recombination method recently developed by Baena-Lopez[67]. The 5' (4302nt) and 3' (2928nt) homology arms were produced from a *tra* BAC (BAC-PAC resources: CH322-140P01) with the following primer pairs respectively: 5'-AAAAGCGGCCGCCATTCTACTCTTGAATTGGCTAGC-3'/5'-AAAAGTACCATGATGCACTTTCCTCAGTGTGA-3' and 5'-AAAAGGCGCGCCAAGAGAATACCATGG-3'/5'-AAAAGGCGCGCCATTGTCGACACAATCAAACTG-3'. PCRs were performed with Q5 high-fidelity polymerase from New England Biolabs (M0491S). The PCR products were digested with NotI/KpnI or AscI respectively prior to cloning into the pTV^{Cherry} vector to generate pTV^{Cherry}[tra]. The vector was sequence-verified and inserted into random genomic locations by P-element-mediated transformation (Bestgene). Transformants (not necessarily mapped or homozygosed) were crossed to *hs-FLP, hs-SceI* flies (DBSC: 25679) and the resulting larvae were heat-shocked at 48, 72, 96 and 120 hrs after egg laying for 1 hr at 37°C. Approximately 200 adult females with mottled eyes (indicating the presence of pTV^{Cherry}[tra] and the transgenes carrying hs-FLP and hs-SceI) were crossed in pools of 15 to *ubiquitin-Gal4[3xP3-GFP]* males and the progeny was screened for the presence of red-eyed flies. The *ubiquitin-Gal4[3xP3-GFP]* transgene was subsequently removed by selecting against the presence of GFP in the ocelli. The generated deletion removed 342 nucleotides starting 13 nucleotides upstream of the transcription start site.

Generation of the UAS-$msl\text{-}2^{HA}$ line

To overexpress *msl-2*, a transgenic *UAS* line was generated from *msl-2* cDNA adding an HA tag at the C-terminal (BDGP Gold cDNAs, clone ID: GH22488) with the following primer pair: 5'-AAA AAGATCTATGGCTCAGACGGCATACTTG and 5'-AAAATCTAGATTAAGCGTAATCTGGAACATCGTATGGGTACAAGTCATCCGAGCCC GAC-3'. PCR was performed with Q5 high-fidelity polymerase from New England Biolabs (M0491S). The PCR product was digested with BglII and XbaI prior to cloning into the *pUASTattb* vector[68]. The construct was sequence-verified and a transgenic line was established through ΦC-31 integrase mediated transformation (Bestgene, attP site ZH-86Fb, DBSC: 24749).

Immunohistochemistry

Intact guts were fixed at room temperature for 20 min in PBS, 3.7% formaldehyde. All subsequent incubations were done in PBS, 4% horse serum, 0.2% Triton X-100 at 4°C following standard protocols.

The following primary antibodies were used: mouse anti-Sxl (M114, DSHB Hydridoma) 1/50, mouse anti-Sxl (M18, DSHB Hydridoma) 1/50, goat anti-Msl-2 (dC-20, sc-32459, Santa Cruz Biotechnology) 1/50, chicken anti-beta galactosidase (ab9361, Abcam) 1/200, rabbit anti-phospho-Histone H3 Ser10 (9701L, Cell Signalling Technology) 1/500, rabbit anti-fru^{M} (Male-2, generated by [69]) 1/500, mouse anti-Dsx^{DBD} (DSHB Hybridoma) 1/100, mouse anti-Prospero (MR1A, DSHB Hybridoma) 1/50, goat anti-ac-Histone H4 Lys16 (sc-8662, Santa Cruz Biotechnology) 1/ 500, rat anti-HA (11867423001, Roche) 1/500, mouse anti-GFP (11814460001, Roche) 1/1000, mouse anti-Pdm1 (kind gift of Steve Cohen, generated by [70]) 1/20. Fluorescent secondary antibodies (FITC-, Cy3- and Cy5-conjugated) were obtained from Jackson Immunoresearch. Vectashield with DAPI (Vector Labs) was used to stain DNA.

Cell, clone and midgut length quantifications

Mitotic indices were quantified by counting phospho-Histone H3-positive cells in >10 midguts per genotype, time point, and/or condition (e.g. male/female), and are displayed as means ± standard error of the mean (SEM). For posterior midgut cell counts, a midgut portion immediately anterior to the junction with the tubules and hindgut was imaged at 20× magnification. Cells were counted using ImageJ in areas of identical size across all genotypes to control for size differences. Threshold was adjusted for the GFP channel (ImageJ function: Image>Adjust>Threshold) to subtract background, and the percentage of area above the threshold were considered (ImageJ function: analyse particles). Data was collected from at least 10 midguts per genotype and/or condition, and is displayed as mean of % of GFP-positive area ± SEM.

MARCM clones were quantified as number of cells per clone (when the GFP reporter was expressed in the nucleus) or by the size of the GFP area/clone (in arbitrary units, when the reporter was membrane-tagged GFP).

To measure midgut length, guts were dissected and were then straightened on polyLysine-coated slides. After imaging, a line was draw between the most anterior point of the proventriculus and the midgut-hindgut junction using ImageJ. The number of pixels contained in the line was used as a proxy for midgut length. For display purposes, the value obtained for a control female midgut selected at random was used as reference to normalise all the other values, which are shown as percentage of control female length value.

Functional RNAi screen of *tra* targets

To test the functional significance of *tra* targets, only those with female/*tra* null mutant female fold differences in transcript abundance >±2 that were also under *tra* control in adult intestinal progenitors were selected for functional validation. The contribution of these *tra* targets to sex differences in adult ISC proliferation was investigated using publicly available *RNAi* and *UAS* lines (see below for details of the RNAi lines, and Methods section ‘Fly stocks’ for details of the UAS lines) expressed from $esg\text{-}Gal4^{ts}$. Results obtained with 11 out of the 16 lines belonging to the VDRC KK collection were not considered and are not shown in Extended Data Fig. 7 because their expression in adult ISCS from $esg^{TS}\text{-}Gal4$ resulted in a recurrent ISC differentiation phenotype in both males and females. We attribute this effect

Europe PMC Funders Author Manuscripts

to the previously reported dominant *Gal4*-dependent toxicity issue with this VDRC KK collection[71]).

Gene	Transformant ID	Library
Idgf1	12416	GD
Snp88Eb	28425	GD
CG17470	100414	KK
CG8008	4159	GD
Klp54D	100140	KK
CG4500	34852	GD
CG4500	106260	KK
Arr1	22196	GD
Arr1	109860	KK
Arr1		UAS
rdo	107213	KK
rdo		UAS
Spn47C	25534	GD
Spn47C	105933	KK
Cyp12d1-p	49269	GD
Cyp12d1-p	109256	KK
TwdlE	24867	GD
TwdlE	107483	KK
Cyp12d1-d	109248	KK
Cyp12d1-d	50507	GD
GstE2	32945	GD
GstE4	100986	KK
GstE4	20472	GD
GstE4		UAS
lectin-28C	45634	GD
lectin-28C	104290	KK
AANATL2	44677	GD
AANATL2	102802	KK
CG5348	1698	GD
CG5348	106565	KK
CG15128	100238	KK
CG15128	19302	GD
CG15236	101045	KK
Ir10a	45403	GD
Ir10a	100181	KK

Statistics and data presentation

All statistical analyses were carried out in the R environment[72]. Comparisons between two genotypes/conditions were analyzed with the Mann-Whitney-Wilcoxon rank sum test (R

function wilcox.test). All graphs were generated using Adobe Illustrator. All confocal and bright field images belonging to the same experiment and displayed together in our figure were acquired using the exact same settings. For visualization purposes, level and channel adjustments were applied using ImageJ to the confocal images shown in the figure panels (the same correction was applied to all images belonging to the same experiment), but all quantitative analyses were carried out on unadjusted raw images or maximum projections. In all figures, n denotes the number of midguts, ISCs/EBs, mitoses or clones that were analysed for each genotype. Values are presented as average ± standard error of the mean (SEM), p-values from Mann-Whitney-Wilcoxon test (non-significant (ns): $p>0.05$; *: $0.05>p>0.01$; **: $0.01>p>0.001$; ***: $p>0.001$). Lines and asterisks highlighting significant comparisons across sexes are displayed in red, whereas those highlighting significant comparisons within same-sex datasets are displayed in black.

RNA-seq experiments

RNA extraction—RNA from 30 pooled dissected midguts was extracted using Trizol (Invitrogen), and 3 such samples were used for each sex and genotype. RNA-seq libraries were prepared from 500ng of total RNA using the Illumina Truseq mRNA stranded library prep kit (Illumina Inc. San Diego, USA) according to the manufacturer's protocol. Library quality was checked on a Bioanalyser HS DNA chip and concentrations were estimated by Qubit measurement. Libraries were pooled in equimolar quantities and sequenced on a Hiseq2500 using paired end 100bp reads. At least 30 million reads passing filter were achieved per sample. After demultiplexing, raw RNASeq reads were aligned with Tophat splice junction mapper[73], version 2.0.11 against Ensembl *Drosophila* genome reference sequence assembly (dm3) and transcript annotations.

For differential gene expression analysis, gene-based read counts were then obtained using HTSeq count module (version 0.5.3p9)[74]. Differential expression analysis was performed on the counts data using DESeq2 Bioconductor package[75]. The analysis was run with the default parameters. DESeq2 package uses negative binomial model to model read counts and then performs statistical tests for differential expression of genes. Raw p values were then adjusted for multiple testing with the Benjamini-Hochberg procedure. GO enrichment analysis was performed using FlyMine v40.1.b. In Fig. 3a, b and Extended Data Fig. 1g, each column corresponds to one of three different replicates (30 midguts each) for each sex, and transcript abundance for each gene was normalized to a scale of −2 (white) to +2 (gray).

Isoform expression analysis—Reads were first aligned to the transcript sets using Bowtie software (version 1.0.0)[76]. Transcript annotations for cDNA and non-coding RNAs were obtained from Ensembl (release 75). Isoform abundances were then calculated using mmseq R package (version 1.0.8)[77]. Differential expression analysis was performed on these abundances using the DESeq2 Bioconductor package (version 1.42.1)[78]. Isoforms not expressed in any of the samples were not included in the differential expression analysis. Raw p values were adjusted for multiple testing with the Benjamini-Hochberg procedure. Initial isoform analysis identified differential expression for 1379 isoforms between male and female midguts ($p<0.05$ cutoff), which, following subtraction of those corresponding to single-isoform genes, yielded 704 isoforms (see main text for subsequent analysis).

Europe PMC Funders Author Manuscripts

RNA-seq data displays—For the volcano plots in Extended Data Fig. 1, log 2 fold change values were plotted against log 10 of adjusted p values. Genes and isoforms significantly upregulated in males are coloured blue, while those significantly upregulated in females are coloured red. Selected genes and isoforms are further highlighted as empty circles. For the scatter charts with quadrants in Extended Data Fig. 7, log 2 fold change values (between control and *tra* mutant females) were plotted against log 2 fold change values (between *tra* mutant females and *tra* mutant females and female with adult-specific, progenitor-specific *tra* expression). Genes and isoforms significantly repressed by *tra* are coloured blue, whereas those significantly activated by *tra* are coloured red. Selected genes and isoforms are further highlighted as empty circles. Volcano plots and scatter charts were generated using Adobe Illustrator. To generate the heat maps, a matrix containing the relative values of gene/isoform expression was built. Transcript abundance for each gene/isoform was normalized to a scale ranging from −2 to +2. A hierarchical clustering algorithm (with Euclidian distance and average linking) was applied to the matrix using the MeV software suite[79]. Area-proportional Venn diagrams were generated using BioVenn (http://www.cmbi.ru.nl/cdd/biovenn/).

Real time qRT-PCRs

RNAs were extracted from 30 dissected midguts using Trizol (Invitrogen). RNAs were cleaned using RNAeasy mini Kit (QIAGEN), and cDNAs were synthesized using the iScript cDNA synthesis kit (Bio-Rad) from 300ng of total RNAs. Quantitative PCRs were performed by mixing cDNA samples (5ng) with iTaq™ Universal SYBR® Green Supermix (Bio-Rad, #172-5124) and the relevant primers in a 96-well plate. Expression values were normalized to eIF4G. For each gene/isoform, at least 3 independent biological replicates were used, and 2 technical replicates were performed. See Supplementary Information for a list of all primers used.

Europe PMC Funders Author Manuscripts

Extended Data

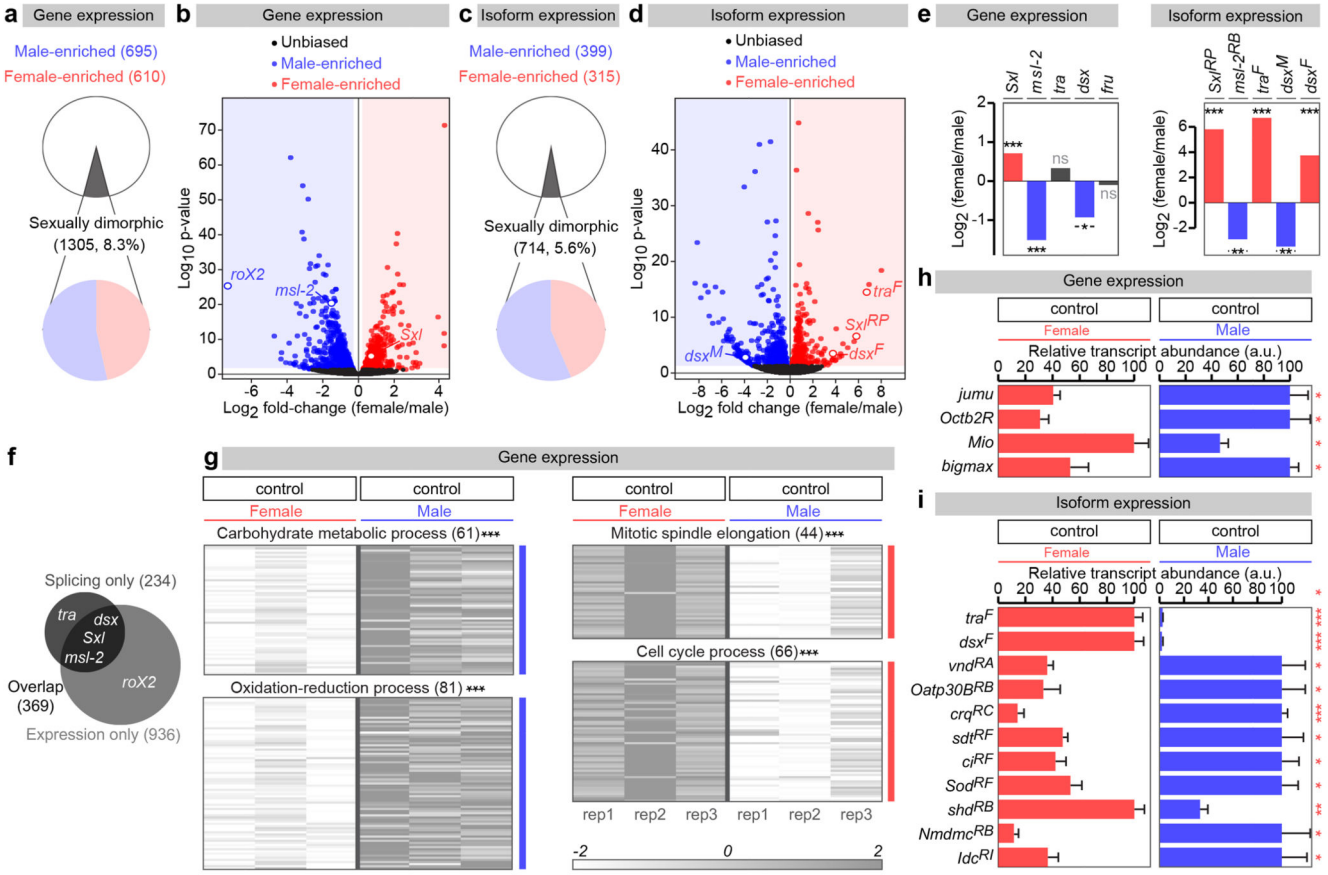

Extended Data Fig. 1. Sexually dimorphic transcription and splicing in the adult midgut

a, Number and percentage of genes with sexually dimorphic gene expression, as revealed by RNA-seq transcriptional profiling of virgin male and female dissected midguts ($p<0.05$ cutoff). **b**, Volcano plot displaying all genes with detectable midgut expression. Female/male ratio of gene expression is shown on the X axis (in log2 scale) and significance is displayed on the Y axis as the negative logarithm (log10 scale) of the adjusted p-value. Genes with significantly upregulated ($p<0.05$ cutoff) expression in males and females are coloured in blue and red, respectively. Other genes are displayed in black. Genes with known sex-specific transcription are displayed as red (female-enriched) or blue (male-enriched) open circles. **c** and **d**, Comparable analyses for sex-biased isoforms belonging to genes with multiple transcripts. We identity 714 sex-biased isoforms belonging to a total of 603 genes. Isoforms resulting from known sex-specific alternative splicing are displayed as in panel **b**. **e**, Female/male ratios of overall transcript abundance (left graph) and abundance of sex-biased isoforms (right graph) for the members of the *Drosophila* sex determination pathway as revealed by RNA-seq analysis of the adult midgut. We note a sexual dimorphism in *dsx* transcript levels. **f**, Venn diagram illustrating the overlap between the genes showing sex-biased expression (overall transcript abundance, light grey, 1305 genes) and sex-biased alternative splicing (sex-biased isoforms, dark grey, 603 genes) in the adult midgut. Known members of the sex determination pathway are displayed as examples. **g**, Heat maps

displaying genes with sexually dimorphic expression clustered by enrichment in specific biological processes, as revealed by Gene Ontology enrichment analysis. Genes with sexually dimorphic expression belonging to the top 4 enriched biological processes are shown. **h** and **i**, Real-time qRT-PCR data for a subset of genes for which RNA-seq transcriptional profiling experiments revealed sexually dimorphic expression (**h**) or isoforms (**i**). RNA was obtained from midguts from virgin male and female samples (same genotypes as for the RNA-seq experiments). For each gene/isoform, expression abundance was arbitrarily set up at 100% for the sex with the highest expression level, and percentage of that expression is displayed for the other sex. See Methods for details, GutSexRNAseq.xls for a full list of names and quality scores, and Supplementary Information for full genotypes.

Europe PMC Funders Author Manuscripts

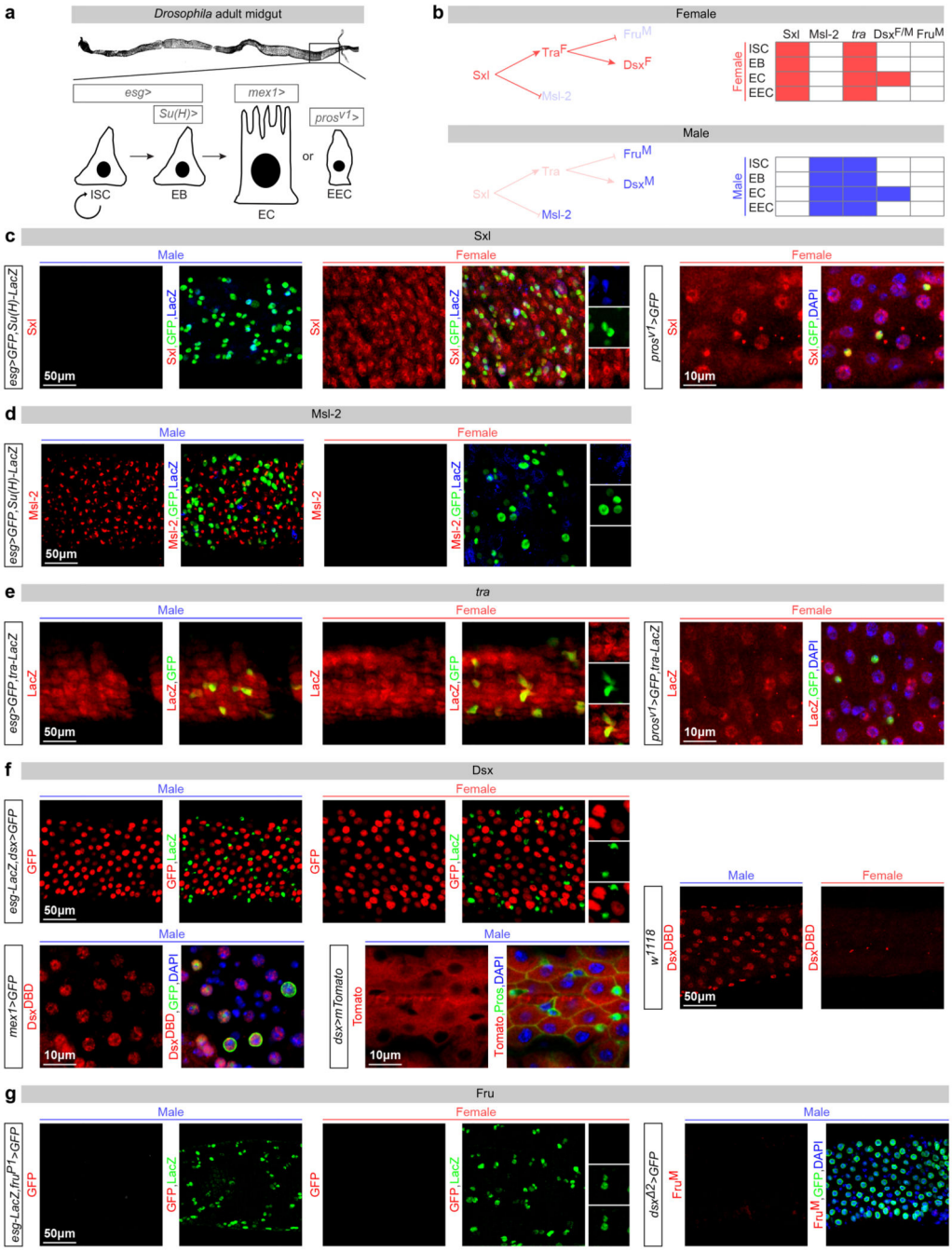

Extended Data Fig. 2. Cell type-specific expression of sex determinants in the adult intestinal epithelium of virgin flies

a, In the adult *Drosophila* midgut, resident stem cells (ISCs) and their postmitotic daughter cells (EBs) maintain the adult intestinal epithelium during normal homeostasis and regenerate it after injury by giving rise to two types of differentiated progeny: ECs and EECs[80,81]. The posterior midgut area used to visualise and quantify phenotypes is boxed. The following *Gal4* drivers were used to label and/or genetically manipulate these four different cell types present in the adult intestinal epithelium: *midgut expression 1 (mex1)* for

Europe PMC Funders Author Manuscripts

ECs, *prospero* (*pros*^{V1}) for EECs, *escargot* (*esg*) to target both ISCs and EBs, and *Supressor or Hairless* (*Su(H)*) for EBs alone. **b**, The canonical sex determination pathway in somatic cells of *Drosophila melanogaster*, consisting of a cascade of sex-specific alternative splicing events culminating in the production of sex-specific transcription factors encoded by Dsx and Fru^{M}. In females, Sex lethal (Sxl) is activated and regulates the splicing of *transformer* (*tra*) pre-mRNA, resulting in the production of Tra^{F}. Tra^{F} regulates the female-specific splicing of *dsx* pre-mRNA (*dsx*^{F}) and *fru* transcript coming from the P1 promoter (*fru*^{P1}, giving rise to *fru*^{M}). In males, Sxl is not expressed and no functional Tra is produced, resulting in default splicing of *dsx* and *fru* pre-mRNAs, leading to Fru^{M} and Dsx^{M} proteins, respectively. The resulting male- and female-specific Dsx and Fru isoforms confer sexual identity to the cells in which they are produced. In addition, in females, Sxl represses dosage compensation by inhibiting Msl-2 expression. The tables summarize the cell-specific expression profiles of the sex determinants in adult midguts of virgin males and females, shown in the panels below. **c**, Sxl protein (in red) is expressed only in female midguts. Co-staining with ISC/EB reporters indicates that Sxl is found *esg*-positive progenitors (ISCs: GFP-positive and LacZ-negative cells, and EBs: GFP-positive and LacZ-positive cells). It is also expressed in female polyploid ECs (GFP- (in green) and LacZ- (in blue) negative cells). Co-staining with *pros*^{V1} reporter indicates that it is also expressed in EECs. **d**, Msl-2 protein is found in the same cell types only in males (staining is confined to the X chromosome, consistent with the signal observed in non-intestinal tissues[82]. **e**, A new reporter of *tra* promoter activity (*tra*^{LacZ}, see Methods for details) is broadly expressed in the epithelium of both male and female midguts, including ISCs and EBs (as revealed by co-staining with *esg-Gal4*-driven GFP) and ECs (GFP-negative cells with large nuclei). Co-staining with *pros*^{V1} reporter indicates that it is also expressed in EECs. **f**, A *dsx-Gal4* reporter (visualised with a GFP reporter that has been false-coloured in red for consistency with the other panels) is active in male and female polyploid ECs (LacZ-negative cells), and is inactive in *esg*-positive progenitors (LacZ-positive cells, in green). Dsx protein (visualised using a Dsx^{DBD}-specific antibody in red) is expressed strongly only in males bot not females, indicating that the sexual dimorphism in *dsx* transcript levels found in our RNA-seq analyses (Extended Data Fig. 1e) is further enhanced at the protein level. Co-staining of the same antibody with the EC marker *mex1-Gal4* confirms expression in ECs. Cytoplasmic *dsx-Gal4*-driven expression of an mTomato reporter is apparent in ECs (visualised as large cells by co-staining with the membrane-enriched marker Armadillo), but is absent from EECs (as revealed by the gaps in mTomato expression in cells that are labelled with Pros). **g**, The *fru*^{P1}*-Gal4* reporter (which labels the only sexually dimorphic *fru* transcript that gives rise to Fru^{M} protein) is inactive in both male and female midguts, as revealed by lack of GFP signal (false-coloured in red for consistency with other panels). Consistent with the lack of *fru*^{P1}*-Gal4* expression, a Fru^{M}-specific antibody (in red) is not expressed in the male midgut. An independent *dsx* reporter (*dsx*$^{\Delta 2}$*-Gal4*) is expressed in polyploid ECs, consistent with the data displayed in **f**. See Supplementary Information for full genotypes.

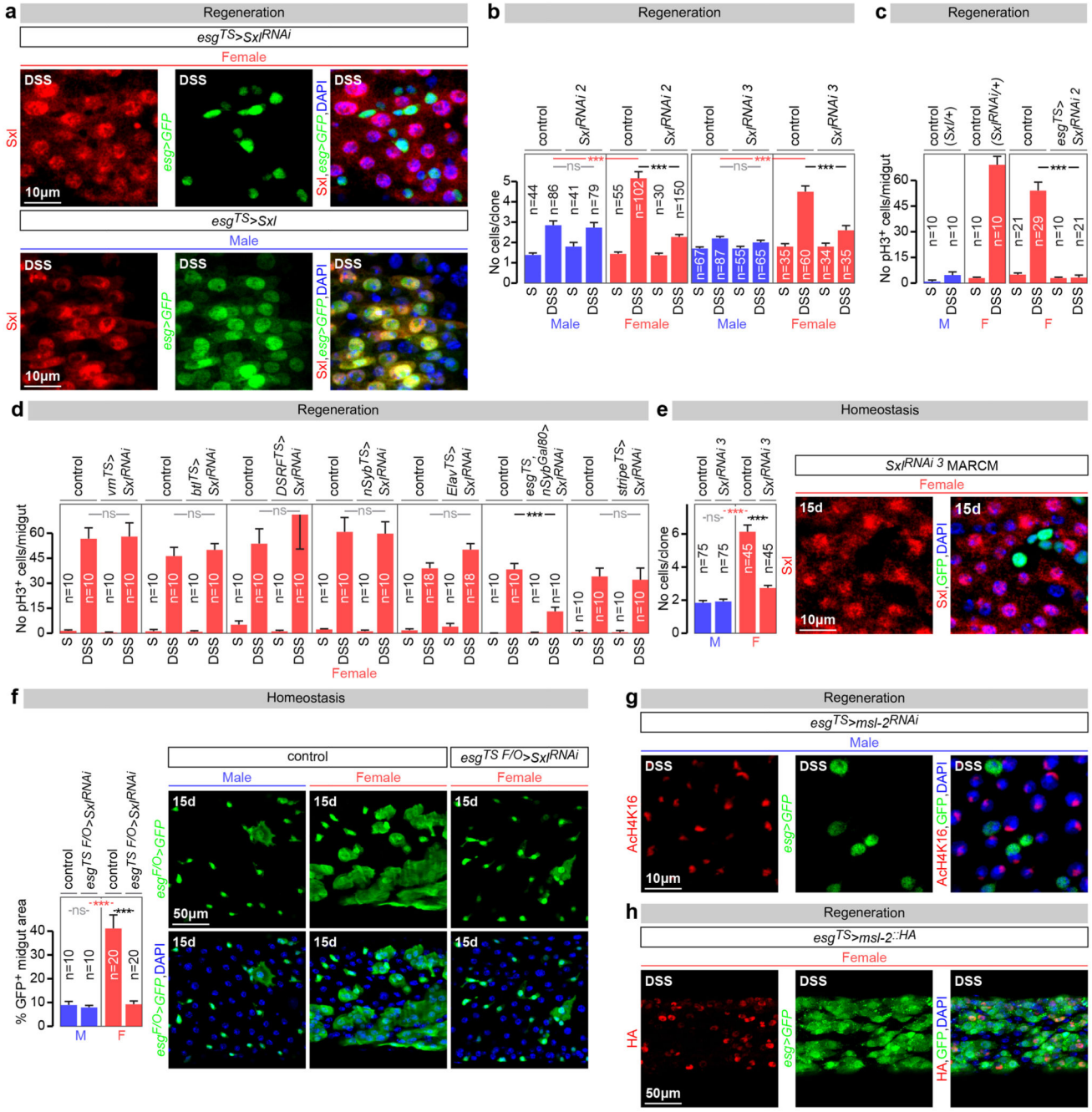

Extended Data Fig. 3. *Sxl* controls intrinsic sex differences in adult ISC proliferation independently of dosage compensation

a, Immunocytochemistry using a Sxl-specific antibody indicates that adult-restricted downregulation of *Sxl* in intestinal progenitors (ISCs/EBs) - achieved by *Gal80*^{TS}-controlled expression of a *Sxl* RNAi transgene – efficiently downregulates Sxl expression in progenitors, but not large polyploid ECs. Conversely, efficient ectopic Sxl protein expression is obtained by expression of a *UAS-Sxl* transgene in adult ISCs/EBs of male flies. In all panels Sxl antibody is in red; DNA: DAPI, in blue; ISC/EB marker: GFP, in green. **b**,

Europe PMC Funders Author Manuscripts

Quantifications of the number of cells inside control MARCM[83] clones, or MARCM clones expressing RNAi transgenes directed against *Sxl* following DSS treatment. 5 days after clone induction by heat shock, female clones are larger than male clones only when *Sxl* is present, confirming the cell autonomy of *Sxl* action. **c**, Additional controls for Fig. 1a, and confirmation of phenotypes using an independent RNAi transgene. This second RNAi transgene against *Sxl* (different from the one used in Fig. 1a) reduces the number of pH3-positive cells in DSS-treated female midguts when expressed from esg^{TS} in adults ISCs/EBs, confirming an adult progenitor-specific requirement for *Sxl* in promoting damage-induced cell divisions in female flies. **d**, Adult-specific downregulation of *Sxl* in adult visceral muscle (using the *vm* driver), trachea (*btl-Gal4* and *DSRF-Gal4*), neurons (*nSyb-Gal4*, *Elav-Gal4*), or fat body (*stripe-Gal4*) does not reduce DSS-induced ISC proliferation in females. By contrast, *Sxl* downregulation using an ISC/EB driver with suppressed neuronal expression (*esg-Gal4* combined with nSyb-Gal80) effectively reduces DSS-induced ISC proliferation in females. Together, these results indicate that *Sxl* does not control sexually dimorphic DSS-induced ISCs proliferation from non-ISC cells. **e**, MARCM clones expressing a third RNAi transgene against *Sxl* (distinct from those used in Fig. 1 and above) are smaller than control clones in females, whereas their size is comparable to that of wild-type or *Sxl-RNAi* clones in males. This confirms that, during normal homeostasis, female ISCs divide more often than male ISCs because of the cell-autonomous action of *Sxl*. The graph shows quantifications of the number of cells within each clone 15 days after clone induction by heat shock, and the confocal images show representative clones (labelled in green with GFP) for each genotype. **f**, Clonal analyses of homeostatic proliferation using the inducible *esg* flip-out system - which labels progenitors and their progeny generated within a defined temporal window[84] - in midguts of control males, control females and females in which *Sxl* downregulation has been confined to adult progenitors. 15 days after induction, the size (assessed as the percentage of GFP-positive area) of control female clones was significantly larger than that of male clones, but both became comparable upon adult-specific *Sxl* downregulation using *Sxl* RNAi transgenes. The graph shows area quantifications for each sex/genotype, and the confocal images show representative clones for each genotype. **g**, Immunohistochemical detection of histone H4 lysine 16 (H4Lys16) acetylation (in red) indicates that adult-specific downregulation of *msl-2* in male intestinal progenitors (ISCs/EBs marker: GFP, in green) results in loss of H4Lys16 acetylation of the X chromosome. **h**, Efficient Msl-2 mis-expression in adult female intestinal progenitors (ISCs/EBs marker: GFP, in green) is confirmed by immunocytochemistry using an HA-specific antibody (in red). n denotes the number of guts (**c**, **d**, **f**), or clones (**b**, **e**) that were analysed for each genotype. Results combined from at least two independent experiments. See Supplementary Information for full genotypes.

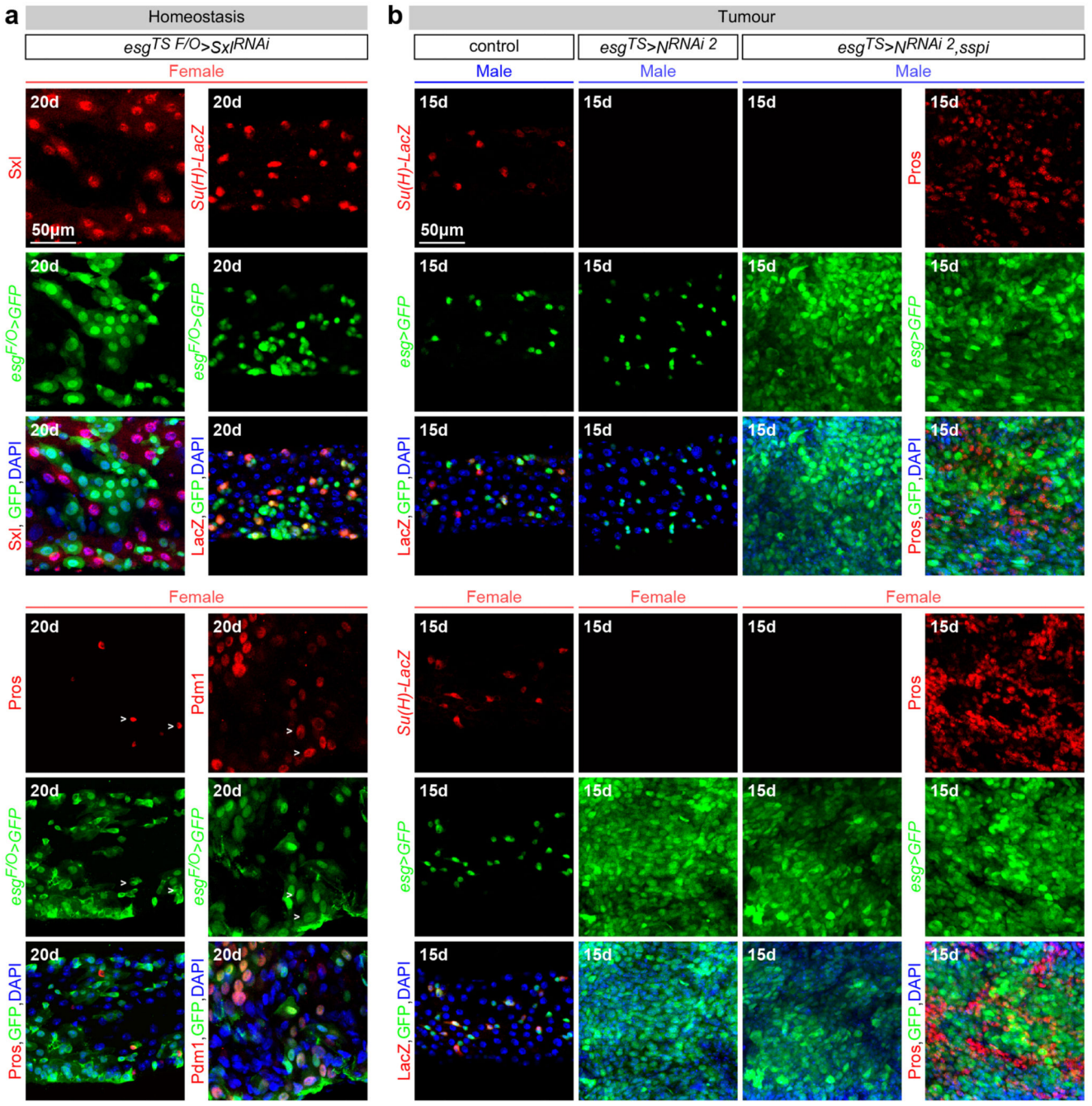

Extended Data Fig. 4. Sexually dimorphic proliferation does not result from sex differences in differentiation

a, Markers for all four intestinal cell types are still apparent following adult-specific downregulation of *Sxl* in the intestinal progenitors of females - achieved by *Gal80^{TS}*-controlled expression of a *Sxl* RNAi transgene. Indeed, expression of *esg-Gal4* (ISC/EBs), *Su(H)-LacZ* (EBs), Pdm1 (ECs) and Pros (EECs) can be readily detected, suggesting that Sxl downregulation in females (which results in reduced ISC proliferation) does not have a major effect on differentiation. Sxl staining confirms efficient downregulation in ISCs/EBs,

but not neighbouring cells. **b**, The same markers reveal that the differentiation defect resulting from *N* downregulation, previously reported in females, is also apparent in males (note loss of *Su(H)-LacZ* following *N* downregulation in both males and females), suggesting that sex differences in differentiation do not contribute to the sex differences in susceptibility to *N*-induced tumours. Co-expression of a mitogen (secreted *Spitz*, *sSpi*) abrogates the sex differences in tumour susceptibility by efficiently triggering hyperplasia also in males, as revealed by an expanded progenitor (GFP-positive) area in both males and females. The identity of these tumours in males is also comparable to that previously show for *N* tumours in females (consisting of high Pros-positive EEC-like cells and low Pros-positive neoplastic ISC-like cells[85]. This further suggests that the sex differences in *N*-induced tumour susceptibility do not arise from sexually dimorphic differentiation effects, but result from sex differences in ISC proliferation. See Supplementary Information for full genotypes.

Europe PMC Funders Author Manuscripts

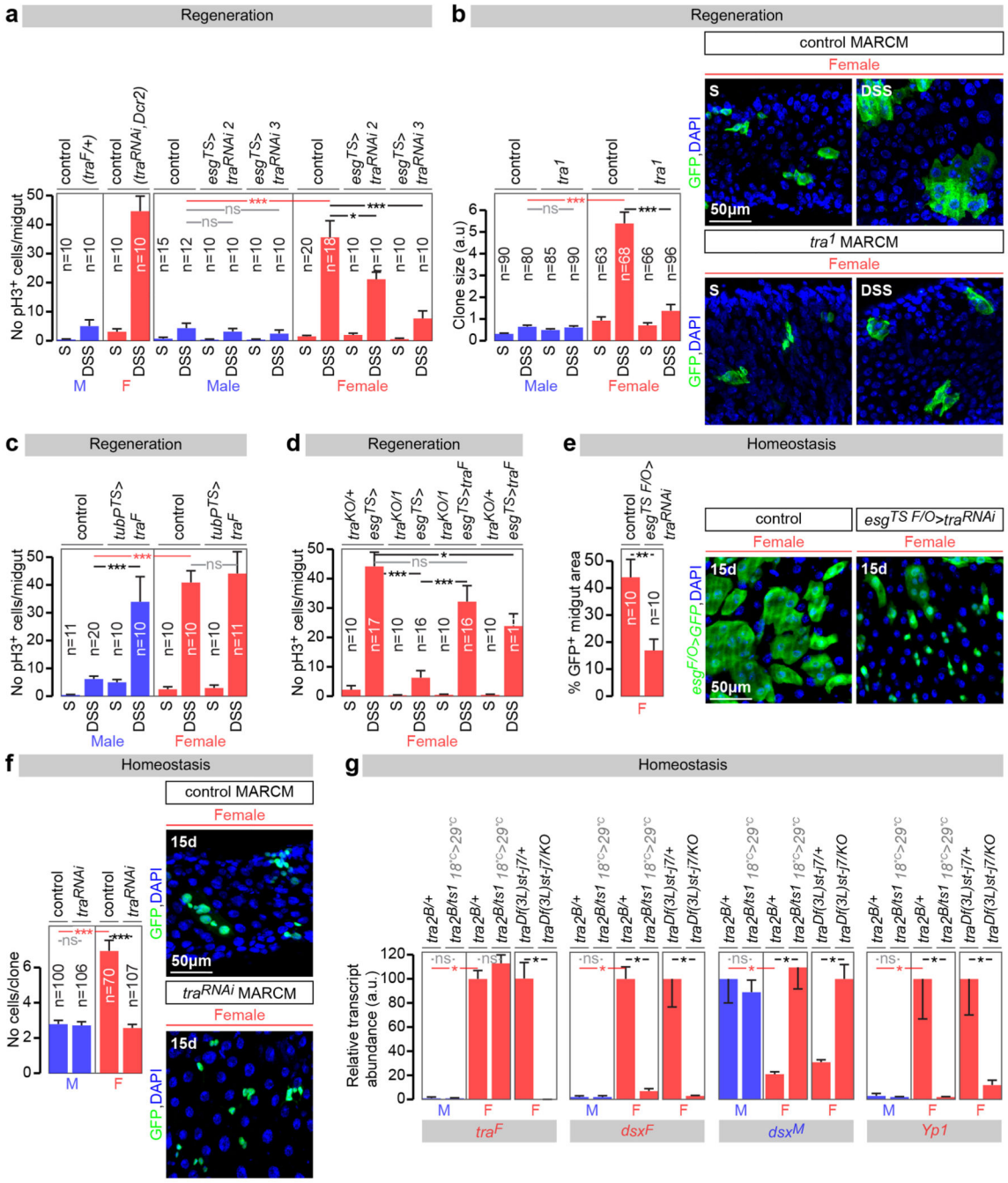

Extended Data Fig. 5. *tra*, but not *tra2*, controls intrinsic sex differences in adult ISC proliferation

a, Additional controls for Fig. 2a, and confirmation of phenotypes using independent RNAi transgenes. Two additional RNAi transgenes against *tra* reduce the number of pH3-positive cells in DSS-treated female – but not male - midguts when expressed from esg^{TS} in adults ISCs/EBs, confirming an adult progenitor-specific requirement for *tra* in promoting damage-induced cell divisions in female flies. **b**, tra^{1} MARCM mutant clones are smaller than control clones in females, whereas their size is comparable to that of wild-type or tra^{1} clones

Europe PMC Funders Author Manuscripts

in males. This confirms that, during normal homeostasis, female ISCs divide more often than male ISCs because of the cell-autonomous action of *tra*. The graph shows quantifications of clone size (in arbitrary units of GFP fluorescence, as described in Methods) 15 days after clone induction by heat shock, and the confocal images show representative clones (labelled in green with GFP) for each genotype. **c**, Ubiquitous, adult-restricted tra^{F} expression from $tubP^{TS}$ in males increases the number of pH3-positive cells following DSS treatment to levels comparable to those of female flies. **d**, Re-introduction of this tra^{F} transgene specifically in adult ISCs/EBs rescues the reduced, male-like intestinal proliferation (as assessed by the number of pH3-positive cells) of *tra* null mutant females entirely lacking the *tra* gene from all their tissues (tra^{KO}/tra^{1}) to levels comparable to those of control females. Expression of this transgene in control heterozygous female flies ($tra^{KO}/+$ esg^{TS}>*traF*) does not significantly increase their proliferation (in fact, it reduces it slightly relative to $tra^{KO}/+$ esg^{TS}> controls, likely as a consequence of its over-expression). **e**, Clonal analyses of homeostatic proliferation using the inducible *esg* flip-out system - which labels progenitors and their progeny generated within a defined temporal window[84] - in midguts of control females and females in which *tra* downregulation has been confined to adult progenitors. 15 days after induction, the size (assessed as the percentage of GFP-positive area) of control clones is significantly larger than that of *tra-RNAi* clones. The graph shows area quantifications for each genotype, and the confocal images show representative clones for each genotype. **f**, Consistent with the *tra* mutant clonal analysis in Fig. 2c, quantifications of clone size (number of cells per clone) reveal that MARCM clones in which *tra* has been downregulated are smaller than control clones only in females. Their size is comparable to that of wild-type or *tra*-downregulated mutant clones in males. The confocal images show representative clones (labelled in green with GFP) for each genotype in females. **g**, qRT-PCR quantifications of relative abundance of tra^{F}, dsx^{F}, dsx^{M} and *Yp1* transcripts in adult-specific *tra2* mutants ($tra2^{B/ts1}$ grown at permissive temperatures, then switched to the restrictive temperature 4 days after eclosion and transcriptionally profiled following 10 additional days at the restrictive temperature) and controls ($tra2^{B}/+$). In *tra2* mutant females, dsx^{F} is lost, dsx^{M} is upregulated to levels comparable to those of control males and *Yp1* (a Dsx^{F} target) is lost (to levels also comparable to those of males). *tra* mutants ($tra^{Df(3L)st-j7/KO}$) were also used as a positive control. n denotes the number of guts (**a**, **c**, **d**, **e**), or clones (**b**, **f**) that were analysed for each genotype. Results combined from at least two independent experiments. See Supplementary Information for full genotypes.

Europe PMC Funders Author Manuscripts

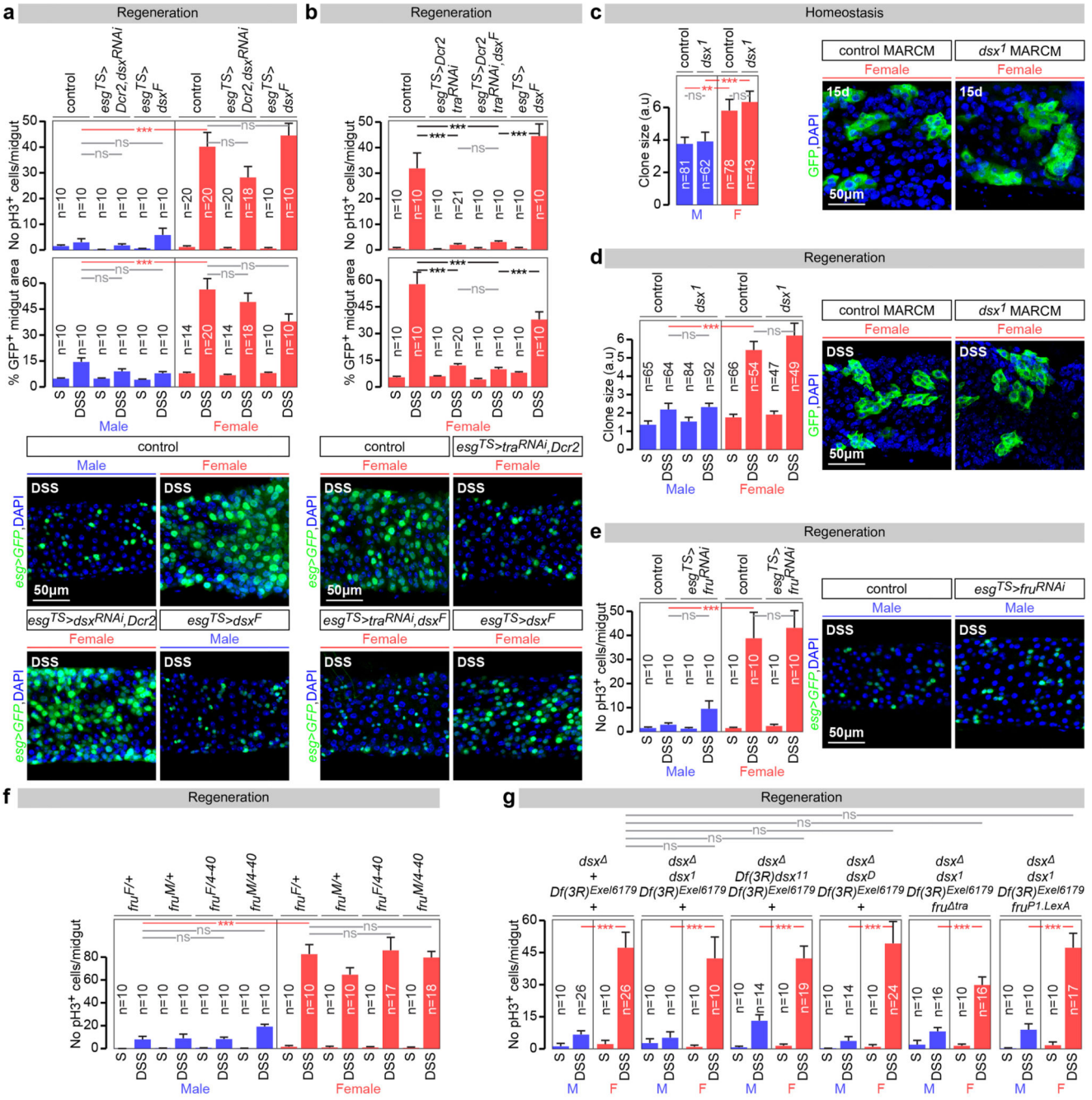

Extended Data Fig. 6. *dsx*- and *fru*^{M}-independent control of sexually dimorphic proliferation in adult intestinal stem cells

a, Adult-restricted downregulation of *dsx* (achieved by co-expression of a *dsx-RNAi* transgene and Dicer-2 (*Dcr-2*) in ISCs/EBs) has no effect on the compensatory ISC proliferation observed upon DSS treatment in neither males nor females. *dsx*^{F} expression in the same conditions does not increase ISC proliferation in either males or females**. b**, *dsx*^{F} expression does not rescue the reduced proliferation resulting from *tra* downregulation in females. Representative images for each genotype are shown in both **a** and **b** (DNA: DAPI,

Europe PMC Funders Author Manuscripts

in blue; ISC/EB marker: GFP, in green). **c**, The size of *dsx* null mutant (dsx^{1}) MARCM clones (quantified in arbitrary units of GFP fluorescence as described in Methods) is comparable to that of controls in both sexes 15 days after clone induction by heat shock. Confocal images show representative clones (labelled in green with GFP) for each genotype. **d**, Quantifications of clone size in control and *dsx* null mutant (dsx^{1}) MARCM clones in the midguts of DSS-treated males and females. 5 days after clone induction by heat shock, there are no significant differences in clone size (quantified in arbitrary units of GFP fluorescence as described in Methods) between control and mutants clones in either males or females. Confocal images show representative clones (labelled in green with GFP) for each genotype. **e**, An RNAi transgene against *fru* does not reduce the number of pH3-positive cells in DSS-treated midguts when expressed from esg^{TS} in the adult ISCs/EBs of either males or females. Confocal images show that number of intestinal progenitors (*esg*-positive cells in green) is also unaffected by this manipulation. **f**, Quantifications of the number of pH3-positive cells upon DSS treatment indicates that the sexual dimorphism in ISC proliferation is unaffected in females with forced fru^{M} expression ($fru^{M}/fru^{4\text{-}40}$) or in males with forced fru^{F} expression ($fru^{F}/fru^{4\text{-}40}$). **g**, ISC proliferation is unaffected in the migduts of DSS-treated males and females entirely lacking *dsx* (dsx^{Δ}/dsx^{1}), producing only Dsx^{F} (dsx^{Δ}/dsx^{11}) or Dsx^{M} (dsx^{Δ}/dsx^{D}). ISC proliferation is also unaffected in *dsx*, fru^{M} double null mutant males and females (dsx^{Δ},$Df(3R)^{Exel6179}/dsx^{1}$, $fru^{P1.LexA}$), and in *dsx* null mutants in which fru^{M} is ectopically produced in females (dsx^{Δ},$Df(3R)^{Exel6179}/dsx^{1}$, $fru^{\Delta tra}$). n denotes the number of guts (**a**, **b**, **e**, **f**, **g**), or clones (**c**, **d**) that were analysed for each genotype. Results combined from at least two independent experiments. See Supplementary Information for full genotypes.

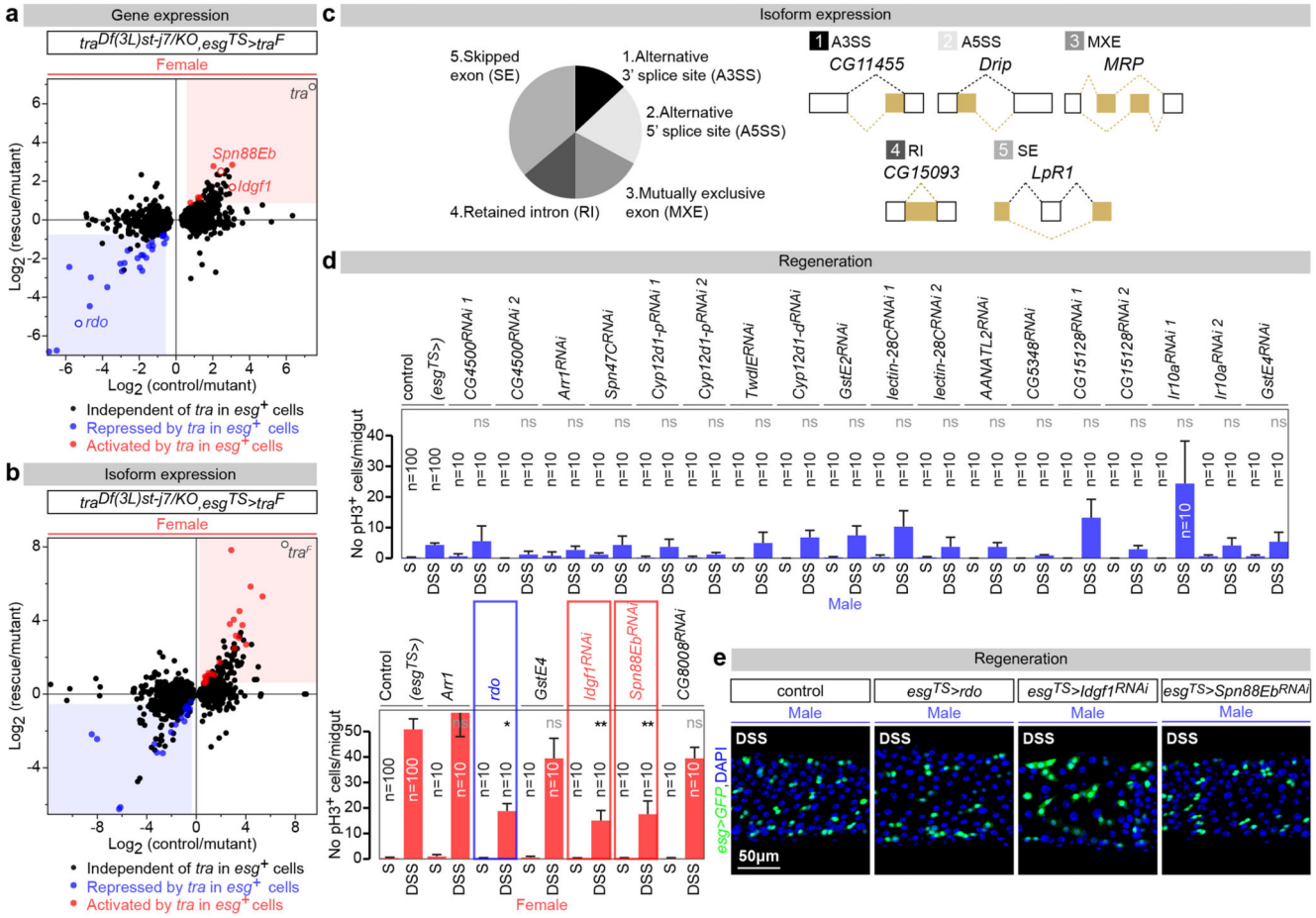

Extended Data Fig. 7. *tra* targets in adult ISCs

a, Scatter plot of all 1346 genes with *tra*-dependent expression in the adult fly midgut. For each gene, control female/*tra* null mutant female ($Df(3L)^{st\text{-}j7}/tra^{KO}$) fold differences in transcript abundance (X axis, log2 scale) are plotted against *tra* mutant female with feminized ISCs (adult-restricted rescue of tra^F in ISCs/EBs)/*tra* mutant female fold differences (Y axis, log2 scale). Genes with *tra*-sensitive expression and significantly repressed by tra^F in ISC/EBs ($p<0.05$ cutoff) are therefore found in the left-bottom quadrant and are displayed in blue, whereas those significantly activated by tra^F are found in the top-right quadrant and are displayed in red. Genes with *tra*-dependent transcription, independent of the action of tra^F in intestinal precursors are displayed in black. **b**, Comparable analysis of *tra*-dependent alternative splicing. **c**, *tra* expression in adult ISCs affects splicing of 38 transcripts by at least 5 different mechanisms. The outcome of each of the alternative splicing mechanisms is shown in yellow for a representative gene. **d**, Adult-restricted downregulation (*RNAi* lines) or mis-expression (*UAS* lines) of *tra* targets in adult ISCs/EBs by means of *esg-Gal4, tubGal80*^{TS}. Genes normally repressed in female progenitors in a tra^F-dependent manner were downregulated in males (top row) and/or misexpressed in females (bottom row). Genes upregulated in female progenitors in a tra^F-dependent manner were downregulated in females (bottom row). Adult-restricted downregulation of *Idgf1 and Spn88Eb* reduces the number of mitoses (pH3-positive cells) in DSS-treated females.

Europe PMC Funders Author Manuscripts

Conversely, *rdo* mis-expression inhibits DSS-induced ISC proliferation in females. Adult-restricted downregulation of other tra^F targets in the same conditions does not affect ISC proliferation in either males or females. **e**, Male controls for Fig. 3c. In contrast to their effects on females, adult ISC/EB-restricted mis-expression of *rdo* or downregulation of *Idgf1 and Spn88Eb* does not reduce the percentage of midgut area covered by *esg*-positive cells in DSS-treated males (DNA: DAPI, in blue; ISC/EB marker: GFP, in green). n denotes the number of guts (**d**) that were analysed for each genotype. Results combined from at least two independent experiments. See Supplementary Information for full genotypes.

Europe PMC Funders Author Manuscripts

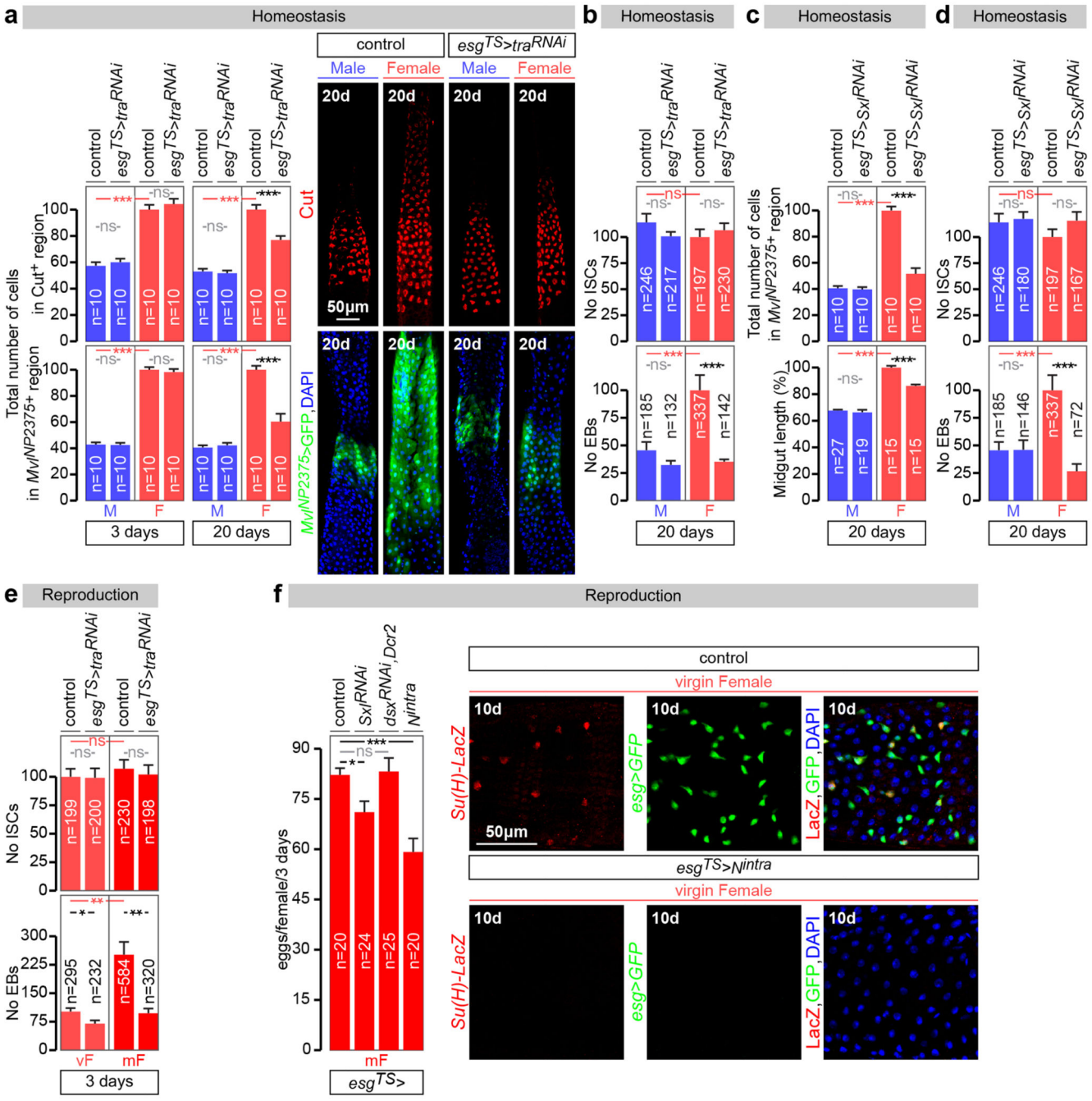

Extended Data Fig. 8. Effects of the sexual identity of adult ISCs on midgut size and reproductive plasticity

a, The number of cells in the R3a-b and R4a midgut regions, defined by expression of Cut and *Mvl*^{NP2375} respectively (as described in [86]), is higher in females, and can be significantly reduced in females to numbers comparable to those found in males after 20 (but not 3) days of adult-specific downregulation of *tra* in intestinal progenitors (achieved by *esg*^{TS}-driven *tra* downregulation initiated after the phase of midgut post-eclosion growth, see Methods for details). No effects are apparent following downregulation in males.

Representative images of these midgut regions (labelled in red with Cut or in green with Mvl^{NP2375},esg^{TS}–driven GFP) are shown to the right for each genotype. **b,** Adult ISC/EB-specific *tra* downregulation does not affect the number of ISCs (*esg*-positive, *Su(H)*-negative cells) in either males or females, but strongly reduces EB (*esg*-positive, *Su(H)*-positive cells) production in females. **c** and **d**, Quantifications as in **a** and **b** for midguts with adult-specific downregulation of *Sxl* in intestinal progenitors. **c**, Reduced number of cells in the R4a midgut region (top graph) and total midgut length (bottom graph) in female flies following 20 days of adult-specific and cell-autonomous masculinization of their intestinal progenitors (achieved by-down regulation of *Sxl* over 20 days with *esg-Gal4*). The same manipulation has no discernible effects in males. **d**, The same genetic manipulation does not affect the number of ISCs (*esg*-positive, *Su(H)*-negative cells) in either males or females, but strongly reduces EB (*esg*-positive, *Su(H)*-positive cells) production in females. **e**, The number of EBs (*esg*-and *Su(H)*-positive cells, bottom graph), but not ISCs (*esg*-positive only cells, top graph) is higher in control female flies 3 days after mating. Adult ISC/EB-specific *tra* downregulation abrogates the postmating increase in EBs in females without affecting EB number in males, or ISC number in males or females. **f**, Adult-specific *Sxl* downregulation in intestinal progenitors leads to a small, but significant, reduction in egg production. An unrelated manipulation that also reduces ISC proliferation by inducing differentiation of ISCs (esg^{TS}>$Notch^{intra}$, images to the right of the graph and [87]) also results in reduced egg production, whereas downregulation of *dsx* (which does not control sex differences in progenitor proliferation) has no such effect. It should, however, be noted that *esg-Gal4* is expressed in a subset of cells in the ovary niche[21]. Hence, the possibility that these cells contribute to the observed phenotype cannot entirely be ruled out. Images to the right show loss of intestinal progenitor cell makers *esg-Gal4* and *Su(H)-LacZ* following expression of N^{intra} in adult intestinal progenitors, indicative of loss of progenitor identity. n denotes the number of guts (**a**, **c**), ISCs/EBs (**b**, **d, e**), or female flies (**f**) that were analysed for each genotype. Results combined from at least two independent experiments. See Supplementary Information for full genotypes.

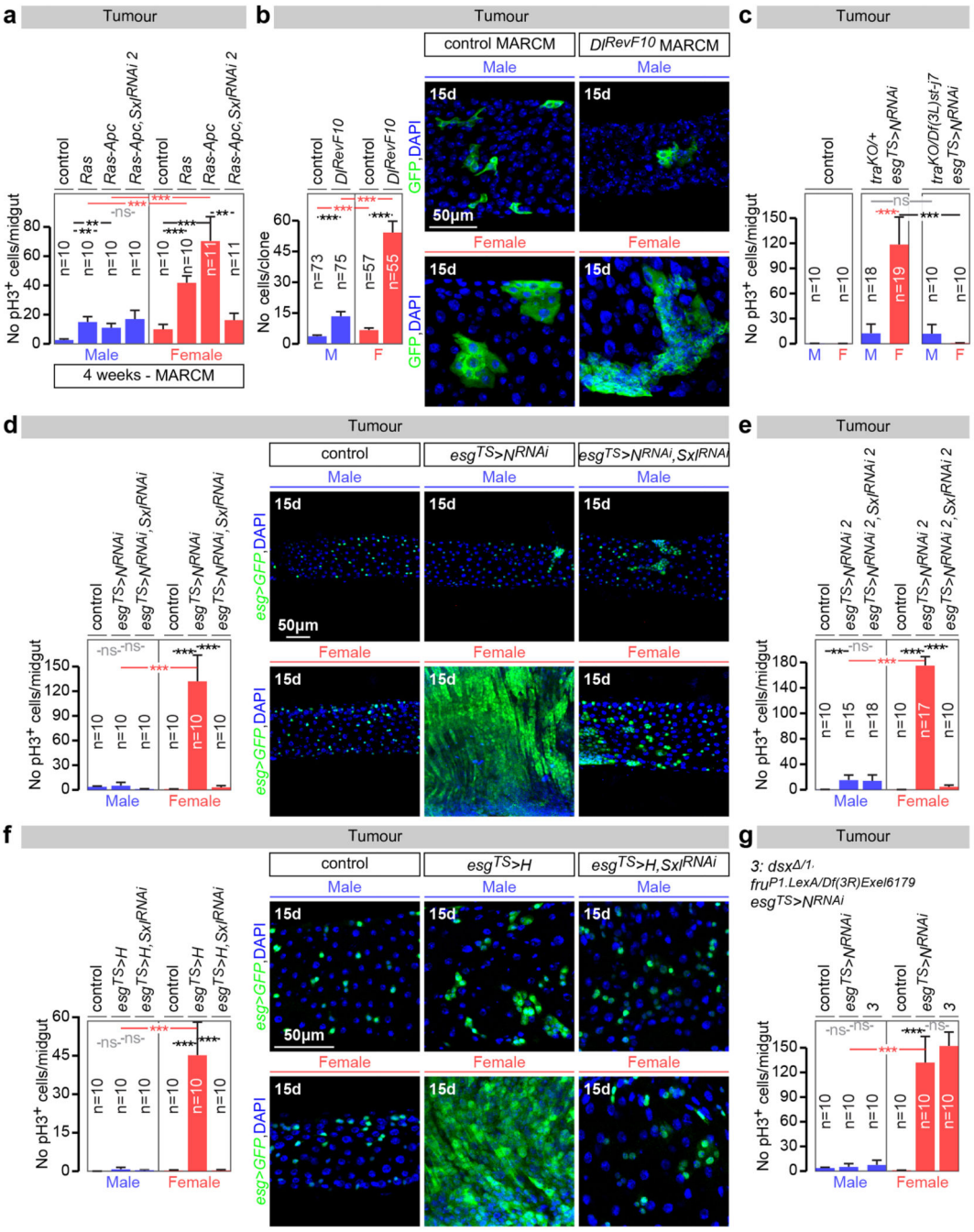

Extended Data Fig. 9. Effects of the sexual identity of adult ISCs on the susceptibility to genetically induced tumours

a, The number of mitoses in *Apc-ras* mutant midguts is larger than that of control clones in both sexes, but it is higher and dependent on *Sxl* in females. **b**, The size of *Delta* (*Dl*, the *N* ligand) null mutant (Dl^{RevF10}) MARCM clones is larger than that of control clones in both sexes, but female mutant clones are larger than male mutant clones. The graph shows quantifications of the number of cells within each clone 15 days after clone induction by heat shock, and the confocal images show representative clones (labelled in green with GFP)

Europe PMC Funders Author Manuscripts

for each genotype. **c**, In *tra* "female" mutant flies (tra^{KO} and $tra^{KO}/Df(3L)^{st\text{-}j7}$) reduced *N* signalling in intestinal progenitors fails to induce the hyperplasia (quantified by the number of pH3 cells) normally observed in control females. **d**, Following 15 days of adult-specific downregulation of *Notch* (N) in intestinal progenitors, hyperplasia (quantified by the number of pH3-positive cells and also shown in representative images) is observed in female, but not male midguts. Adult-specific and cell-autonomous reversal of ISC/EB female identity – achieved by esg^{TS}-driven downregulation of *Sxl* – fully prevents the hyperplasia induced by *Notch* downregulation in females, but has no effects on males. Confocal images show intestinal progenitor coverage of representative midgut portions for each genotype (DNA: DAPI, in blue; ISC/EB marker: GFP, in green). **e**, pH3 quantifications show a comparable effect for an independent RNAi transgene against *Sxl*. **f**, Adult-specific downregulation of *Notch* (N) signalling by ectopic expression of the downstream *N* signalling antagonist *Hairless* (*H*)[38] leads to hyperplasia (quantified by the number of pH3-positive cells and also shown in representative images) in female, but not male midguts. Adult-specific and cell-autonomous reversal of ISC/EB female identity – achieved by esg^{TS}-driven downregulation of *Sxl* – fully prevents the hyperplasia induced by *H* overexpression in females, but has no effects on males. Confocal images show intestinal progenitor coverage of representative midgut portions for each genotype (DNA: DAPI, in blue; ISC/EB marker: GFP, in green). **g**, The number of pH3-positive cells 15 days after *N* downregulation in adult intestinal progenitors of double null mutant flies lacking *dsx* and fru^{M} (dsx^{Δ},$Df(3R)^{Exel6179}/dsx^{1}$, $fru^{P1.LexA}$) is comparable to that of controls in both males and female flies. Like control flies, it is significantly higher in female flies. Virgin flies were used in all these experiments. n denotes the number of guts (**a**, **c**, **d**, **e**, **f**, **g**), or clones (**b**) that were analysed for each genotype. Results combined from at least two independent experiments. See Supplementary Information for full genotypes.

Supplementary Material

Refer to Web version on PubMed Central for supplementary material.

ACKNOWLEDGEMENTS

We thank Konstantinos Vanezis and Laurence Game for technical assistance, and Cayetano Gonzalez, Tom Carroll and Daniel Perea for discussions. Bruce Baker, Allison Bardin, Alberto Baena-Lopez, Sarah Bray, Andreu Casali, Thomas Cline, Steve Cohen, Daniel Eberl, Stephen Goodwin, Greg Jefferis, Leanne Jones, Ryusuke Niwa, Benjamin Prud'homme, Iris Salecker, Lucas Sanchez, Carl Thummel, Jessica Treisman, Marcos Vidal, Daisuke Yamamoto and Laurence Zwiebel shared reagents. Dafni Hadjieconomou, Jake Jacobson, George King and Esmeralda Parra-Peralbo provided comments on the manuscript. This work was funded by an ERC Starting Grant to I.M-A. (ERCStG 310411) and MRC intramural funding. B.H. holds an EMBO long-term fellowship and I.M-A. is a member of, and is supported by, the EMBO Young Investigator Programme.

REFERENCES

1. Arnold AP. The end of gonad-centric sex determination in mammals. Trends in genetics : TIG. 2012; 28:55–61. doi:10.1016/j.tig.2011.10.004. [PubMed: 22078126]
2. Ober C, Loisel DA, Gilad Y. Sex-specific genetic architecture of human disease. Nature reviews. Genetics. 2008; 9:911–922. doi:10.1038/nrg2415.
3. Cognigni P, Bailey AP, Miguel-Aliaga I. Enteric neurons and systemic signals couple nutritional and reproductive status with intestinal homeostasis. Cell metabolism. 2011; 13:92–104. doi:10.1016/j.cmet.2010.12.010. [PubMed: 21195352]

4. Lucchesi JC, Kuroda MI. Dosage compensation in Drosophila. Cold Spring Harbor perspectives in biology. 2015; 7 doi:10.1101/cshperspect.a019398.
5. Boggs RT, Gregor P, Idriss S, Belote JM, McKeown M. Regulation of sexual differentiation in D. melanogaster via alternative splicing of RNA from the transformer gene. Cell. 1987; 50:739–747. [PubMed: 2441872]
6. Camara N, Whitworth C, Van Doren M. The creation of sexual dimorphism in the Drosophila soma. Current topics in developmental biology. 2008; 83:65–107. doi:10.1016/S0070-2153(08)00403-1. [PubMed: 19118664]
7. Christiansen AE, Keisman EL, Ahmad SM, Baker BS. Sex comes in from the cold: the integration of sex and pattern. Trends in genetics : TIG. 2002; 18:510–516. [PubMed: 12350340]
8. Villella A, Hall JC. Neurogenetics of courtship and mating in Drosophila. Advances in genetics. 2008; 62:67–184. doi:10.1016/S0065-2660(08)00603-2. [PubMed: 19010254]
9. Amcheslavsky A, Jiang J, Ip YT. Tissue damage-induced intestinal stem cell division in Drosophila. Cell stem cell. 2009; 4:49–61. doi:10.1016/j.stem.2008.10.016. [PubMed: 19128792]
10. Arthur BI Jr. Jallon JM, Caflisch B, Choffat Y, Nothiger R. Sexual behaviour in Drosophila is irreversibly programmed during a critical period. Current biology : CB. 1998; 8:1187–1190. [PubMed: 9799737]
11. Ferveur JF, et al. Genetic feminization of pheromones and its behavioral consequences in Drosophila males. Science. 1997; 276:1555–1558. [PubMed: 9171057]
12. Clough E, et al. Sex- and tissue-specific functions of Drosophila doublesex transcription factor target genes. Developmental cell. 2014; 31:761–773. doi:10.1016/j.devcel.2014.11.021. [PubMed: 25535918]
13. Ma Q, Wawersik M, Matunis EL. The Jak-STAT target Chinmo prevents sex transformation of adult stem cells in the Drosophila testis niche. Developmental cell. 2014; 31:474–486. doi: 10.1016/j.devcel.2014.10.004. [PubMed: 25453558]
14. Matson CK, et al. DMRT1 prevents female reprogramming in the postnatal mammalian testis. Nature. 2011; 476:101–104. doi:10.1038/nature10239. [PubMed: 21775990]
15. Shapiro-Kulnane L, Smolko AE, Salz HK. Maintenance of Drosophila germline stem cell sexual identity in oogenesis and tumorigenesis. Development. 2015; 142:1073–1082. doi:10.1242/dev. 116590. [PubMed: 25758221]
16. Uhlenhaut NH, et al. Somatic sex reprogramming of adult ovaries to testes by FOXL2 ablation. Cell. 2009; 139:1130–1142. doi:10.1016/j.cell.2009.11.021. [PubMed: 20005806]
17. Caldwell JC, Fineberg SK, Eberl DF. reduced ocelli encodes the leucine rich repeat protein Pray For Elves in Drosophila melanogaster. Fly. 2007; 1:146–152. [PubMed: 18820435]
18. Handke B, et al. The hemolymph proteome of fed and starved Drosophila larvae. PloS one. 2013; 8:e67208. doi:10.1371/journal.pone.0067208. [PubMed: 23840627]
19. Kawamura K, Shibata T, Saget O, Peel D, Bryant PJ. A new family of growth factors produced by the fat body and active on Drosophila imaginal disc cells. Development. 1999; 126:211–219. [PubMed: 9847235]
20. Brown JB, et al. Diversity and dynamics of the Drosophila transcriptome. Nature. 2014; 512:393–399. doi:10.1038/nature12962. [PubMed: 24670639]
21. Reiff T, et al. Endocrine remodelling of the adult intestine sustains reproduction in Drosophila. eLife. 2015; 4:e06930. doi:10.7554/eLife.06930. [PubMed: 26216039]
22. Ohlstein B, Spradling A. The adult Drosophila posterior midgut is maintained by pluripotent stem cells. Nature. 2006; 439:470–474. doi:10.1038/nature04333. [PubMed: 16340960]
23. Patel PH, Edgar BA. Tissue design: how Drosophila tumors remodel their neighborhood. Seminars in cell & developmental biology. 2014; 28:86–95. doi:10.1016/j.semcdb.2014.03.012. [PubMed: 24685612]
24. Evans DS, Cline TW. Drosophila switch gene Sex-lethal can bypass its switch-gene target transformer to regulate aspects of female behavior. Proceedings of the National Academy of Sciences of the United States of America. 2013; 110:E4474–4481. doi:10.1073/pnas.1319063110. [PubMed: 24191002]

25. Finley KD, Taylor BJ, Milstein M, McKeown M. dissatisfaction, a gene involved in sex-specific behavior and neural development of Drosophila melanogaster. Proceedings of the National Academy of Sciences of the United States of America. 1997; 94:913–918. [PubMed: 9023356]
26. Robinett CC, Vaughan AG, Knapp JM, Baker BS. Sex and the single cell. II. There is a time and place for sex. PLoS biology. 2010; 8:e1000365. doi:10.1371/journal.pbio.1000365. [PubMed: 20454565]
27. Markle JG, et al. Sex differences in the gut microbiome drive hormone-dependent regulation of autoimmunity. Science. 2013; 339:1084–1088. doi:10.1126/science.1233521. [PubMed: 23328391]
28. Steegenga WT, et al. Sexually dimorphic characteristics of the small intestine and colon of prepubescent C57BL/6 mice. Biology of sex differences. 2014; 5:11. doi:10.1186/s13293-014-0011-9. [PubMed: 25243059]
29. Cook MB, et al. Sex disparities in cancer incidence by period and age. Cancer epidemiology, biomarkers & prevention : a publication of the American Association for Cancer Research, cosponsored by the American Society of Preventive Oncology. 2009; 18:1174–1182. doi:10.1158/1055-9965.EPI-08-1118.
30. Siudeja K, et al. Frequent Somatic Mutation in Adult Intestinal Stem Cells Drives Neoplasia and Genetic Mosaicism during Aging. Cell stem cell. 2015

ADDITIONAL REFERENCES

31. Ruiz MF, Sarno F, Zorrilla S, Rivas G, Sanchez L. Biochemical and functional analysis of Drosophila-sciara chimeric sex-lethal proteins. PloS one. 2013; 8:e65171. doi:10.1371/journal.pone.0065171. [PubMed: 23762307]
32. Lu B, Ackerman L, Jan LY, Jan YN. Modes of protein movement that lead to the asymmetric localization of partner of Numb during Drosophila neuroblast division. Molecular cell. 1999; 4:883–891. [PubMed: 10635314]
33. Zielke N, et al. Fly-FUCCI: A versatile tool for studying cell proliferation in complex tissues. Cell reports. 2014; 7:588–598. doi:10.1016/j.celrep.2014.03.020. [PubMed: 24726363]
34. Ferveur JF, Stortkuhl KF, Stocker RF, Greenspan RJ. Genetic feminization of brain structures and changed sexual orientation in male Drosophila. Science. 1995; 267:902–905. [PubMed: 7846534]
35. Lee G, Hall JC, Park JH. Doublesex gene expression in the central nervous system of Drosophila melanogaster. Journal of neurogenetics. 2002; 16:229–248. [PubMed: 12745633]
36. Merrill CE, Sherertz TM, Walker WB, Zwiebel LJ. Odorant-specific requirements for arrestin function in Drosophila olfaction. Journal of neurobiology. 2005; 63:15–28. doi:10.1002/neu.20113. [PubMed: 15627264]
37. Daborn PJ, et al. Evaluating the insecticide resistance potential of eight Drosophila melanogaster cytochrome P450 genes by transgenic over-expression. Insect biochemistry and molecular biology. 2007; 37:512–519. doi:10.1016/j.ibmb.2007.02.008. [PubMed: 17456446]
38. Bardin AJ, Perdigoto CN, Southall TD, Brand AH, Schweisguth F. Transcriptional control of stem cell maintenance in the Drosophila intestine. Development. 2010; 137:705–714. doi:10.1242/dev.039404. [PubMed: 20147375]
39. de Celis JF, Bray S. Feed-back mechanisms affecting Notch activation at the dorsoventral boundary in the Drosophila wing. Development. 1997; 124:3241–3251. [PubMed: 9310319]
40. Schweitzer R, Shaharabany M, Seger R, Shilo BZ. Secreted Spitz triggers the DER signaling pathway and is a limiting component in embryonic ventral ectoderm determination. Genes & development. 1995; 9:1518–1529. [PubMed: 7601354]
41. Martorell O, et al. Conserved mechanisms of tumorigenesis in the Drosophila adult midgut. PloS one. 2014; 9:e88413. doi:10.1371/journal.pone.0088413. [PubMed: 24516653]
42. Kohl J, Ostrovsky AD, Frechter S, Jefferis GS. A bidirectional circuit switch reroutes pheromone signals in male and female brains. Cell. 2013; 155:1610–1623. doi:10.1016/j.cell.2013.11.025. [PubMed: 24360281]
43. Mellert DJ, Robinett CC, Baker BS. doublesex functions early and late in gustatory sense organ development. PloS one. 2012; 7:e51489. doi:10.1371/journal.pone.0051489. [PubMed: 23240029]

44. Cande J, Stern DL, Morita T, Prud'homme B, Gompel N. Looking under the lamp post: neither fruitless nor doublesex has evolved to generate divergent male courtship in Drosophila. Cell reports. 2014; 8:363–370. doi:10.1016/j.celrep.2014.06.023. [PubMed: 25017068]
45. Baker BS, Hoff G, Kaufman TC, Wolfner MF, Hazelrigg T. The doublesex locus of Drosophila melanogaster and its flanking regions: a cytogenetic analysis. Genetics. 1991; 127:125–138. [PubMed: 1901816]
46. Duncan IW, Kaufman TC. Cytogenic analysis of chromosome 3 in Drosophila melanogaster: mapping of the proximal portion of the right arm. Genetics. 1975; 80:733–752. [PubMed: 811500]
47. Demir E, Dickson BJ. fruitless splicing specifies male courtship behavior in Drosophila. Cell. 2005; 121:785–794. doi:10.1016/j.cell.2005.04.027. [PubMed: 15935764]
48. Mellert DJ, Knapp JM, Manoli DS, Meissner GW, Baker BS. Midline crossing by gustatory receptor neuron axons is regulated by fruitless, doublesex and the Roundabout receptors. Development. 2010; 137:323–332. doi:10.1242/dev.045047. [PubMed: 20040498]
49. Belote JM, Hoffmann FM, McKeown M, Chorsky RL, Baker BS. Cytogenetic analysis of chromosome region 73AD of Drosophila melanogaster. Genetics. 1990; 125:783–793. [PubMed: 2118870]
50. Sturtevant AH. A gene in Drosophila melanogaster that transforms females into males. Genetics. 1945; 30:297–299. [PubMed: 17247159]
51. Mattox W, Baker BS. Autoregulation of the splicing of transcripts from the transformer-2 gene of Drosophila. Genes & development. 1991; 5:786–796. [PubMed: 2026327]
52. Belote JM, Baker BS. Sexual behavior: its genetic control during development and adulthood in Drosophila melanogaster. Proceedings of the National Academy of Sciences of the United States of America. 1987; 84:8026–8030. [PubMed: 3120181]
53. Gowen JW, Fung STC. Determination of sex through genes in a major sex locus in Drosophila melanogaster. Heredity. 1957; 11:397–402.
54. Anand A, et al. Molecular genetic dissection of the sex-specific and vital functions of the Drosophila melanogaster sex determination gene fruitless. Genetics. 2001; 158:1569–1595. [PubMed: 11514448]
55. Haenlin M, Kramatschek B, Campos-Ortega JA. The pattern of transcription of the neurogenic gene Delta of Drosophila melanogaster. Development. 1990; 110:905–914. [PubMed: 2128477]
56. Morel V, Schweisguth F. Repression by suppressor of hairless and activation by Notch are required to define a single row of single-minded expressing cells in the Drosophila embryo. Genes & development. 2000; 14:377–388. [PubMed: 10673509]
57. Furriols M, Bray S. A model Notch response element detects Suppressor of Hairless-dependent molecular switch. Current biology : CB. 2001; 11:60–64. [PubMed: 11166182]
58. Rideout EJ, Dornan AJ, Neville MC, Eadie S, Goodwin SF. Control of sexual differentiation and behavior by the doublesex gene in Drosophila melanogaster. Nature neuroscience. 2010; 13:458–466. doi:10.1038/nn.2515. [PubMed: 20305646]
59. Manoli DS, et al. Male-specific fruitless specifies the neural substrates of Drosophila courtship behaviour. Nature. 2005; 436:395–400. doi:10.1038/nature03859. [PubMed: 15959468]
60. Wang L, Zeng X, Ryoo HD, Jasper H. Integration of UPRER and oxidative stress signaling in the control of intestinal stem cell proliferation. PLoS genetics. 2014; 10:e1004568. doi:10.1371/journal.pgen.1004568. [PubMed: 25166757]
61. Zeng X, Chauhan C, Hou SX. Characterization of midgut stem cell- and enteroblast-specific Gal4 lines in drosophila. Genesis. 2010; 48:607–611. doi:10.1002/dvg.20661. [PubMed: 20681020]
62. Phillips MD, Thomas GH. Brush border spectrin is required for early endosome recycling in Drosophila. Journal of cell science. 2006; 119:1361–1370. doi:10.1242/jcs.02839. [PubMed: 16537648]
63. Balakireva M, Stocker RF, Gendre N, Ferveur JF. Voila, a new Drosophila courtship variant that affects the nervous system: behavioral, neural, and genetic characterization. The Journal of neuroscience : the official journal of the Society for Neuroscience. 1998; 18:4335–4343. [PubMed: 9592110]

64. Pan Y, Robinett CC, Baker BS. Turning males on: activation of male courtship behavior in Drosophila melanogaster. PloS one. 2011; 6:e21144. doi:10.1371/journal.pone.0021144. [PubMed: 21731661]

65. Shiga Y, Tanaka-Matakatsu M, Hayashi S. A nuclear GFP/ beta-galactosidase fusion protein as a marker for morphogenesis in living Drosophila. Dev Growth Differ. 1996; 38:99–106.

66. Misra JR, Horner MA, Lam G, Thummel CS. Transcriptional regulation of xenobiotic detoxification in Drosophila. Genes & development. 2011; 25:1796–1806. doi:10.1101/gad.17280911. [PubMed: 21896655]

67. Baena-Lopez LA, Alexandre C, Mitchell A, Pasakarnis L, Vincent JP. Accelerated homologous recombination and subsequent genome modification in Drosophila. Development. 2013; 140:4818–4825. doi:10.1242/dev.100933. [PubMed: 24154526]

68. Bischof J, Maeda RK, Hediger M, Karch F, Basler K. An optimized transgenesis system for Drosophila using germ-line-specific phiC31 integrases. Proceedings of the National Academy of Sciences of the United States of America. 2007; 104:3312–3317. doi:10.1073/pnas.0611511104. [PubMed: 17360644]

69. Kimura K, Ote M, Tazawa T, Yamamoto D. Fruitless specifies sexually dimorphic neural circuitry in the Drosophila brain. Nature. 2005; 438:229–233. doi:10.1038/nature04229. [PubMed: 16281036]

70. Yeo SL, et al. On the functional overlap between two Drosophila POU homeo domain genes and the cell fate specification of a CNS neural precursor. Genes & development. 1995; 9:1223–1236. [PubMed: 7758947]

71. Green EW, Fedele G, Giorgini F, Kyriacou CP. A Drosophila RNAi collection is subject to dominant phenotypic effects. Nature methods. 2014; 11:222–223. doi:10.1038/nmeth.2856. [PubMed: 24577271]

72. R Development Core Team. R Foundation for Statistical Computing. 2014.

73. Kim D, et al. TopHat2: accurate alignment of transcriptomes in the presence of insertions, deletions and gene fusions. Genome biology. 2013; 14:R36. doi:10.1186/gb-2013-14-4-r36. [PubMed: 23618408]

74. Anders S, Pyl PT, Huber W. HTSeq--a Python framework to work with high-throughput sequencing data. Bioinformatics. 2015; 31:166–169. doi:10.1093/bioinformatics/btu638. [PubMed: 25260700]

75. Anders S, Huber W. Differential expression analysis for sequence count data. Genome biology. 2010; 11:R106. doi:10.1186/gb-2010-11-10-r106. [PubMed: 20979621]

76. Langmead B, Trapnell C, Pop M, Salzberg SL. Ultrafast and memory-efficient alignment of short DNA sequences to the human genome. Genome biology. 2009; 10:R25. doi:10.1186/gb-2009-10-3-r25. [PubMed: 19261174]

77. Turro E, et al. Haplotype and isoform specific expression estimation using multi-mapping RNA-seq reads. Genome biology. 2011; 12:R13. doi:10.1186/gb-2011-12-2-r13. [PubMed: 21310039]

78. Love MI, Huber W, Anders S. Moderated estimation of fold change and dispersion for RNA-seq data with DESeq2. Genome biology. 2014; 15:550. doi:10.1186/s13059-014-0550-8. [PubMed: 25516281]

79. Saeed AI, et al. TM4 microarray software suite. Methods in enzymology. 2006; 411:134–193. doi:10.1016/S0076-6879(06)11009-5. [PubMed: 16939790]

80. Jiang H, Edgar BA. Intestinal stem cell function in Drosophila and mice. Current opinion in genetics & development. 2012; 22:354–360. doi:10.1016/j.gde.2012.04.002. [PubMed: 22608824]

81. Lemaitre B, Miguel-Aliaga I. The digestive tract of Drosophila melanogaster. Annual review of genetics. 2013; 47:377–404. doi:10.1146/annurev-genet-111212-133343.

82. Kelley RL, et al. Expression of msl-2 causes assembly of dosage compensation regulators on the X chromosomes and female lethality in Drosophila. Cell. 1995; 81:867–877. [PubMed: 7781064]

83. Lee T, Luo L. Mosaic analysis with a repressible cell marker for studies of gene function in neuronal morphogenesis. Neuron. 1999; 22:451–461. [PubMed: 10197526]

84. Jiang H, et al. Cytokine/Jak/Stat signaling mediates regeneration and homeostasis in the Drosophila midgut. Cell. 2009; 137:1343–1355. doi:10.1016/j.cell.2009.05.014. [PubMed: 19563763]

85. Patel PH, Dutta D, Edgar BA. Niche appropriation by Drosophila intestinal stem cell tumours. Nature cell biology. 2015; 17:1182–1192. doi:10.1038/ncb3214. [PubMed: 26237646]

86. Buchon N, et al. Morphological and molecular characterization of adult midgut compartmentalization in Drosophila. Cell reports. 2013; 3:1725–1738. doi:10.1016/j.celrep.2013.04.001. [PubMed: 23643535]

87. Micchelli CA, Perrimon N. Evidence that stem cells reside in the adult Drosophila midgut epithelium. Nature. 2006; 439:475–479. doi:10.1038/nature04371. [PubMed: 16340959]

Europe PMC Funders Author Manuscripts

Europe PMC Funders Author Manuscripts

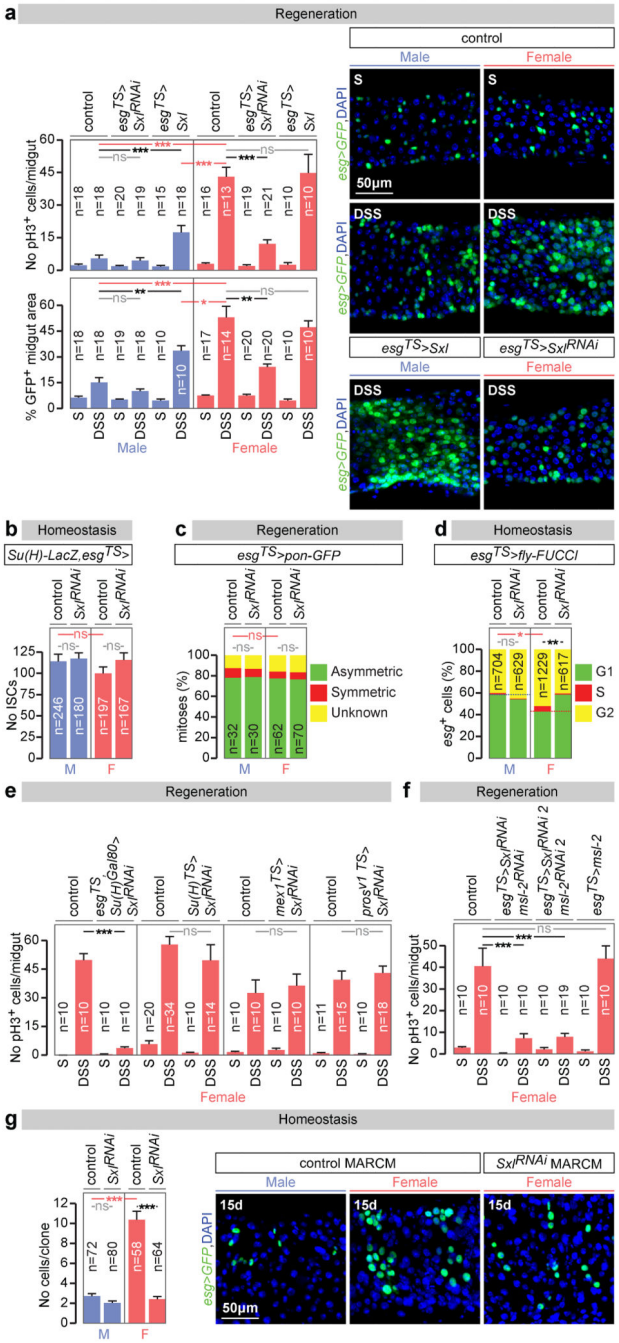

Figure 1. *Sxl* controls intrinsic sex differences in adult ISC proliferation independently of dosage compensation

a, Number of mitoses (phospho-histone H3 (pH3)-positive cells, top graph) and percentage of cells positive for intestinal progenitor markers (escargot (*esg*)-positive/total area, bottom graph) in controls and flies with adult-restricted downregulation or mis-expression of *Sxl* in ISCs/EBs (achieved by *esg-Gal4*, *tub-Gal80*^{TS}-driven *Sxl* RNAi or *UAS-Sxl*, respectively). Flies were exposed to control (sucrose, S) or damage-inducing (DSS) diets. Representative images are shown to the right (DNA: DAPI, in blue; ISC/EB marker: GFP, in green). **b**,

Europe PMC Funders Author Manuscripts

Stem cell number (*esg*$^{+}$, Supressor of Hairless (*Su(H)*)$^{-}$ cells) in the posterior midgut following 20 days of adult ISC/EB-specific *Sxl* downregulation. **c**, Quantifications of symmetric (red) vs asymmetric (green) ISC divisions based on cortical *Partner of Numb (Pon)-GFP* distribution in metaphase and telophase reveal no differences between the sexes or upon adult ISC/EB-specific *Sxl* downregulation. Mitoses with lack of clear *Pon-GFP* signal are displayed in yellow. **d**, Percentage of progenitors in G1, S or G2 as revealed by ISC/EB-driven expression of the cell cycle indicator Fly-FUCCI. **e**, Number of mitoses in DSS-treated flies with adult-specific downregulation of *Sxl* in ISCs (*esg-Gal4*, *Su(H)-Gal80* driver), EBs (*Su(H)-Gal4*), ECs (midgut expression 1 (*mex1-Gal4*) or EECs (prospero (*pros*)^{V1}*-Gal4*). **f**, pH3 quantifications following adult-specific *msl-2* downregulation or mis-expression in ISCs/EBs. **g**, MARCM clone size quantifications (graph) and representative images (labelled in green with GFP) reveal that clones expressing *Sxl-RNAi* are smaller than control clones in females, but not in males. n denotes the number of midguts (**a**, **e**, **f**), ISCs/EBs (**b**, **d**), mitoses (**c**) or clones (**g**) that were analysed for each genotype. Results combined from at least two independent experiments. See Supplementary Information for full genotypes. In this and all subsequent figures, error bars correspond to standard error of the mean (SEM).

Europe PMC Funders Author Manuscripts

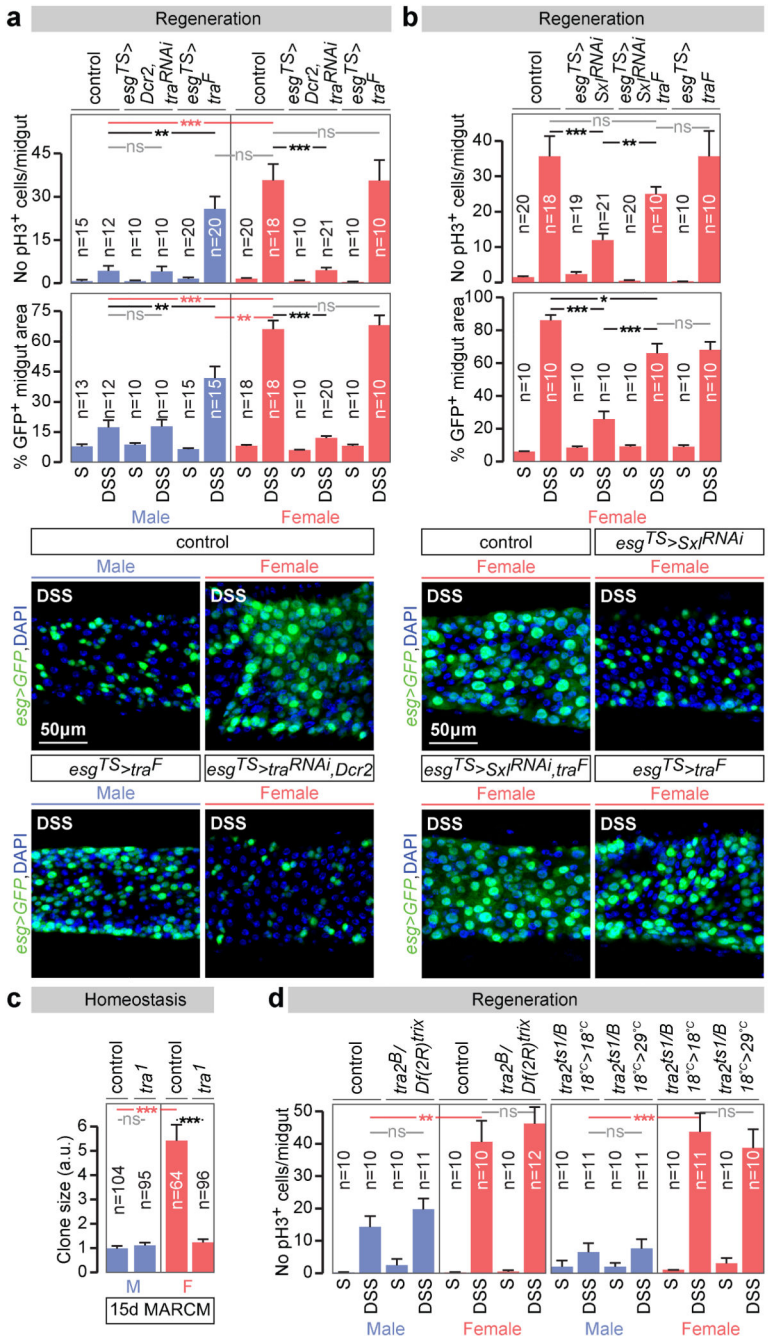

Figure 2. *tra*, but not *tra2*, controls intrinsic sex differences in adult ISC proliferation

a, Mitoses (top graph) and intestinal progenitor area (bottom graph) in flies exposed to control (sucrose, S) or damage-inducing (DSS) diets, in both controls and flies with adult ISC/EB-restricted *tra* downregulation or mis-expression. Representative images are shown below the graphs (DNA: DAPI, in blue; ISC/EB marker: GFP, in green). **b**, Comparable quantifications of the *Sxl* downregulation phenotypes in females, and their rescue by re-expression of tra^F. **c**, Clone size quantifications (in arbitrary units of GFP fluorescence, see Methods) reveal that *tra* null mutant MARCM clones are smaller than control clones only in

females. **d**, No significant differences in ISC proliferation in the midguts of DSS-treated males or females lacking *tra2* (*tra2*$^{B/Df(2R)trix}$), or lacking *tra2* specifically in adults (achieved by shifting flies with the thermosensitive allele *tra2*^{ts1} from 18°C to 29°C in the adult stage), vs controls. n denotes the number of midguts (**a**, **e**, **f**), ISCs/EBs (**b**, **d**), mitoses (**c**) or clones (**g**) that were analysed for each genotype. Results combined from at least two independent experiments. See Supplementary Information for full genotypes.

Europe PMC Funders Author Manuscripts

Europe PMC Funders Author Manuscripts

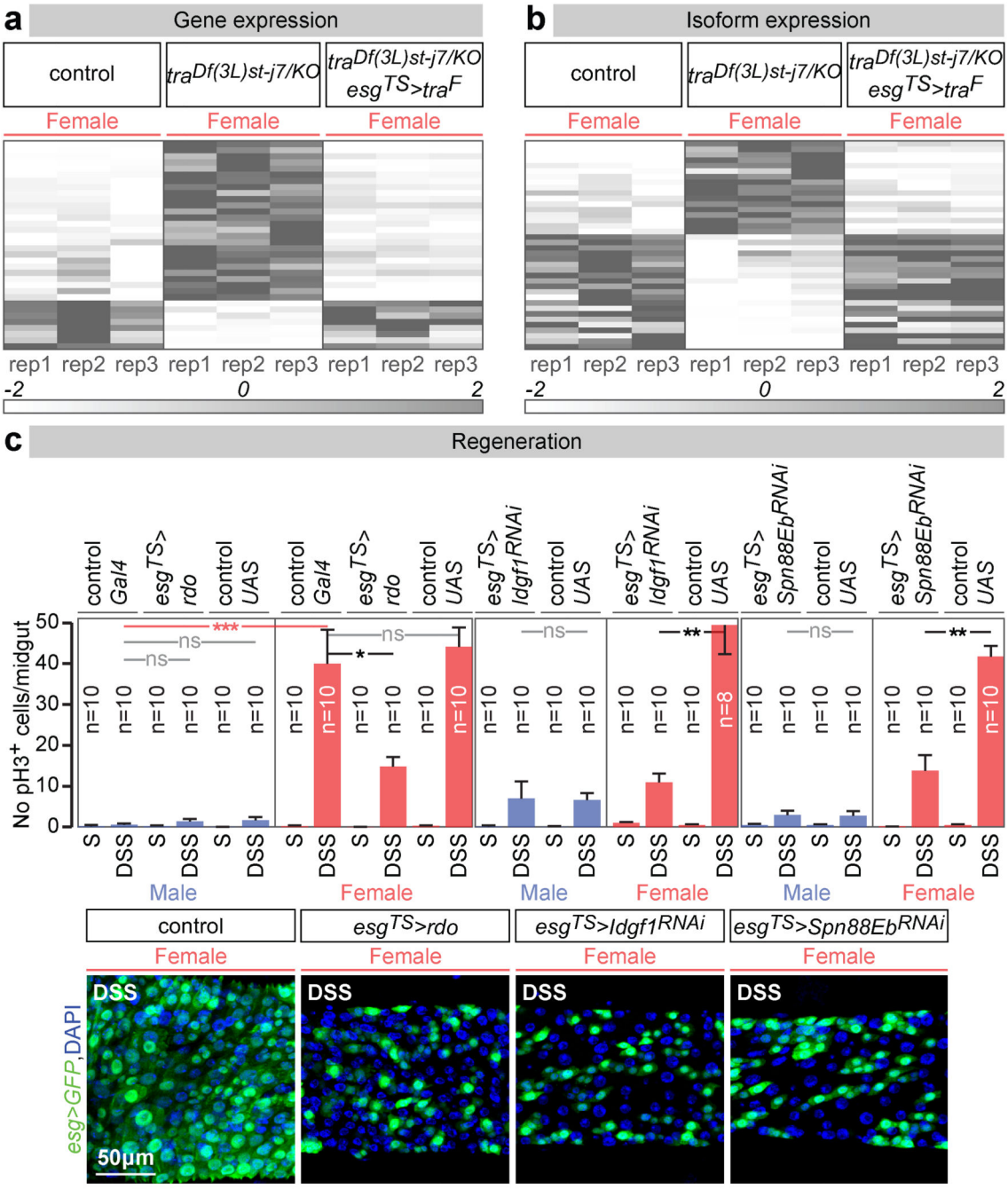

Figure 3. *tra* targets in adult intestinal progenitors

Heat maps of the genes with *tra*-regulated expression (**a**) or splicing (**b**) in ISCs/EBs, displaying their normalized abundance in females, *tra* null mutant females and *tra* null mutant females with feminized ISCs/EBs ($esg^{TS}>tra^{F}$) (see Methods for details). **c**, Mitoses (pH3) quantifications of adult ISC/EB-confined manipulations of *rdo*, *Idgf1* and *Spn88Eb* expression. Representative images for each genotype are shown below the graphs (DNA: DAPI, in blue; ISC/EB marker: GFP, in green). n = 10 midguts per genotype/condition. Results combined from at least two independent experiments. See GutSexRNAseq.xls file

for a full list of names and quality scores, and Supplementary Information for full genotypes.

Europe PMC Funders Author Manuscripts

Europe PMC Funders Author Manuscripts

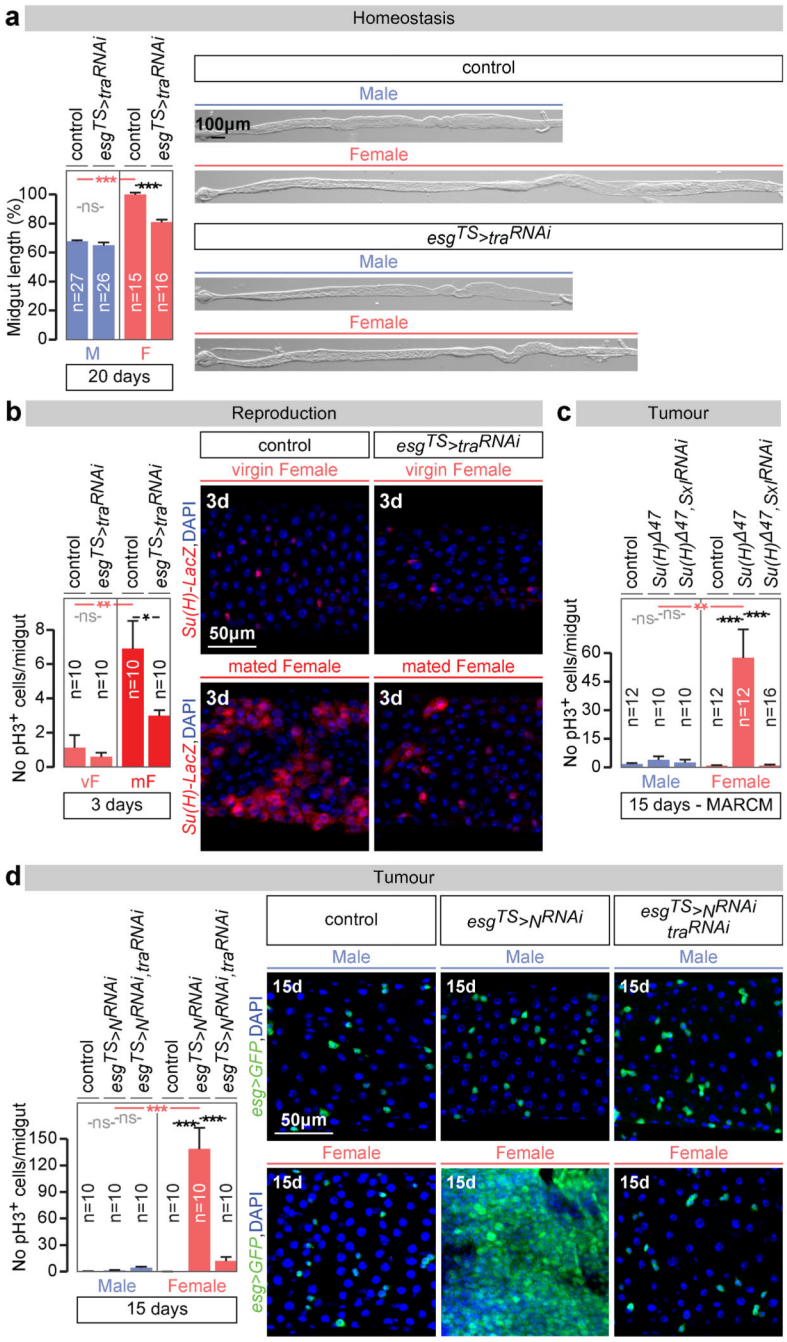

Figure 4. Physiological significance of the sex differences in intestinal progenitors

a, Midgut length quantifications and representative images of phenotypes resulting from adult-specific masculinization of ISC/EB-specific masculinization of ISCs (achieved by *esg*^{TS}-driven *tra* downregulation initiated after the phase of midgut post-eclosion growth, see Methods for details). **b**, The number of mitoses (pH3-positive cells) is higher in control female flies 3 days after mating. The postmating increase is abrogated upon adult ISC/EB-specific *tra* downregulation. An EB marker (*Su(H)LacZ*, in red in image panels) reveals that the EB expansion seen in females after mating is reduced upon adult ISC/EB-specific *tra*

downregulation. See also Extended Data Fig. 8 for quantifications. **c**, pH3 quantifications inside MARCM clones of control flies, *Su(H)* mutants and *Su(H)* mutants in which *Sxl* has been downregulated inside the clone. *Su(H)* mutation only leads to increased pH3 counts in females, and this increase is *Sxl* dependent. **d**, Hyperplasia (quantified by the number of pH3-positive cells) resulting from adult ISC/EB-driven *N* downregulation and its modulation by *tra* in female and male midguts. Confocal images show intestinal progenitor coverage of representative midgut portions for each genotype (DNA: DAPI, in blue; ISC/EB marker: GFP, in green). n denotes the number of midguts (**a**, **b**, **c**, **d**) that were analysed for each genotype. Virgin flies were used in all experiments unless otherwise indicated. Results combined from at least two independent experiments. See Supplementary Information for full genotypes.

Europe PMC Funders Author Manuscripts